J. Fluid Mech. (2005), *vol.* 522, *pp.* 215–252.
DOI: 10.1017/S0022112004001831 Printed in the United Kingdom

Vortex-induced vibrations of a pivoted cylinder

By F. FLEMMING† AND C. H. K. WILLIAMSON

Sibley School of Mechanical and Aerospace Engineering, Upson Hall, Cornell University, Ithaca, NY 14853, USA

(Received 2 March 2004 and in revised form 19 August 2004)

Much of the research into vortex-induced vibrations has been dedicated to the problem of a cylinder vibrating transverse to a fluid flow (Y-motion). There are very few papers studying the more practical case of vibration in two degrees of freedom (XY-motion), or the case where there is variation of amplitude along the span of a body. The present two-degree-of-freedom pivoted cylinder apparatus represents the simplest configuration having a spanwise variation of amplitude. A central question concerns how well the results from Y-motion studies carry over to the case of a body in two degrees of freedom, and also how effective the quasi-uniform assumption is when there is spanwise amplitude variation.

In a manner comparable with the Y-motion cylinder, the principal dynamics of the pivoted body are transverse to the flow. For moderate values of the product: inertia–damping or ($I^*\zeta$), the system exhibits two amplitude response branches, and for sufficiently low ($I^*\zeta$), three response branches appear, in strong analogy with previous results for Y-motion bodies. The response branches for the bodies with low ($I^*\zeta$) correspond with both the 2S mode (two single vortices per cycle) and 2P mode (two vortex pairs per cycle) of vortex formation along the span. We also observe a clear 2S-2P hybrid mode, similar to that found for vibrating tapered cylinders by Techet *et al.* (*J. Fluid Mech.* vol. 363, 1998, p. 79). These different modes correspond well with the Williamson & Roshko (*J. Fluids Struct.* vol. 2, 1988, p. 355) map of modes in the plane of amplitude and frequency, so long as the streamwise vibration is small. However, when the inertia of the body is sufficiently small, the correspondence with the map of modes for the upper branch is not close. The response branches cross over each other in this map, and one has to introduce a third dimension to represent streamwise amplitude. This three–dimensional plot shows that the two response branches exist in quite different parameter spaces. The upper branch with the higher streamwise motion corresponds to a new vortex formation mode, which comprises two co-rotating vortices each half-cycle, defined as a '2C' mode. We present the principal three-dimensional vorticity structures corresponding to each vortex wake mode. Vortex dislocations and vortex merging are characteristics of these complex three–dimensional structures. We introduce equations of motion for the case of the pivoted cylinder with two degrees of freedom, and thereby deduce that a critical inertia, I_{crit} exists analogous to the 'critical mass' of Govardhan & Williamson (*J. Fluid Mech.* vol. 420, 2000, p. 85; vol. 473, 2002, p. 147), below which the pivoted body is predicted to have an infinitely wide regime of flow velocities where resonant oscillations will occur.

---

† Present address: Institute for Energy and Powerplant Technology, Darmstadt University of Technology, Petersenstr. 30, D-64287 Darmstadt, Germany.

1. Introduction

Recently there has been a great deal of practical interest in the problems arising from vortex-induced vibration of structures. Such vibrations occur in many branches of engineering, for example in aeroelastic applications where the fluid is air, yielding mass ratios (m^*) of order 100 (where $m^* =$ mass of oscillating structure/displaced fluid mass), or in hydroelastic applications in water, where m^* is of order 1 or 10. Several reviews discuss these problems (for example, see Sarpkaya 1979; Bearman 1984, and more recently, Williamson & Govardhan 2005). Much research into such vibrations of cylindrical structures has been concerned with motions only transverse to a free stream, because the induced forces due to the vortex dynamics induce motions primarily in that direction. There have been only few studies of a fundamental nature, which probe to what extent the allowance for an elastically mounted body to move in two degrees of freedom will modify the forces, responses and vorticity dynamics of the body in a flow. In most practical cases, cylindrical structures (such as riser tubes or heat exchangers, to name but two examples) have a mass ratio which is the same in both the streamwise (X) and transverse (Y) directions, and these structures have the same natural frequencies in these two directions. There are also very few studies which look into a variation of amplitude along the span of a cylindrical body.

Here, we set out to study the dynamics and vortex formation for a pivoted cylinder, which is able to vibrate in the X- and Y-directions. The pivoted cylinder naturally represents a structure having a linear variation of amplitude along the span. This is perhaps the simplest case of spanwise amplitude variation, and is expected to demonstrate local features generic to other cases of spanwise amplitude variation, such as vibrating cables. We present, in figure 1, some of the cases of fluid–structure interaction which are important to understand, beginning with the paradigm of the 'uniform-amplitude' cylinder. (The terminology 'uniform-amplitude' cylinder is taken to mean the classical case of an elastically mounted cylinder under uniform amplitude vibration, i.e. no spanwise variation.) We include the present pivoted cylinder case, as well as the flexible cantilever (whose dynamics have been studied by Vickery & Watkins 1964; King 1974; and more recently by Pesce & Fujarra 2000; Fujarra *et al.* 2001), and the vibrating cable (see for example, the body and vorticity dynamics computed by Newman & Karniadakis 1996; Evangelinos & Karniadakis 1999; Evangelinos, Lucor & Karniadakis 2000; Lucor, Imas & Karniadakis 2001). Also of distinct relevance is the study of vortex wake modes for an oscillating tapered cylinder by Techet, Hover & Triantafyllou (1998).

For all the above complex flows, we would like to predict structural dynamics. One approach has been to use force data from uniform-amplitude cylinder experiments, compiled for a variation of normalized amplitudes and frequencies. The relevant force (per unit length) data are then matched with the local amplitude and frequency at specific spanwise points, in the case of bodies with spanwise varying amplitudes, such as cantilevers and flexible cables. In this sense, one introduces a 'quasi-uniform' assumption. Of course, there is a feedback between the fluid force and the structural motion: the body responds to the fluid forcing while the forcing depends on the body motion, so the force coefficients must be matched for a converged solution. The present pivoted cylinder is an interesting problem in itself, and there are practical cases involving articulated columns in the ocean, which require knowledge of fluid–structure interaction in the presence of currents. However, this problem also represents an opportunity to study the simplest case of spanwise amplitude variation, and investigate the extent to which the quasi-uniform assumption is capable of predicting the wake vortex modes along the span.

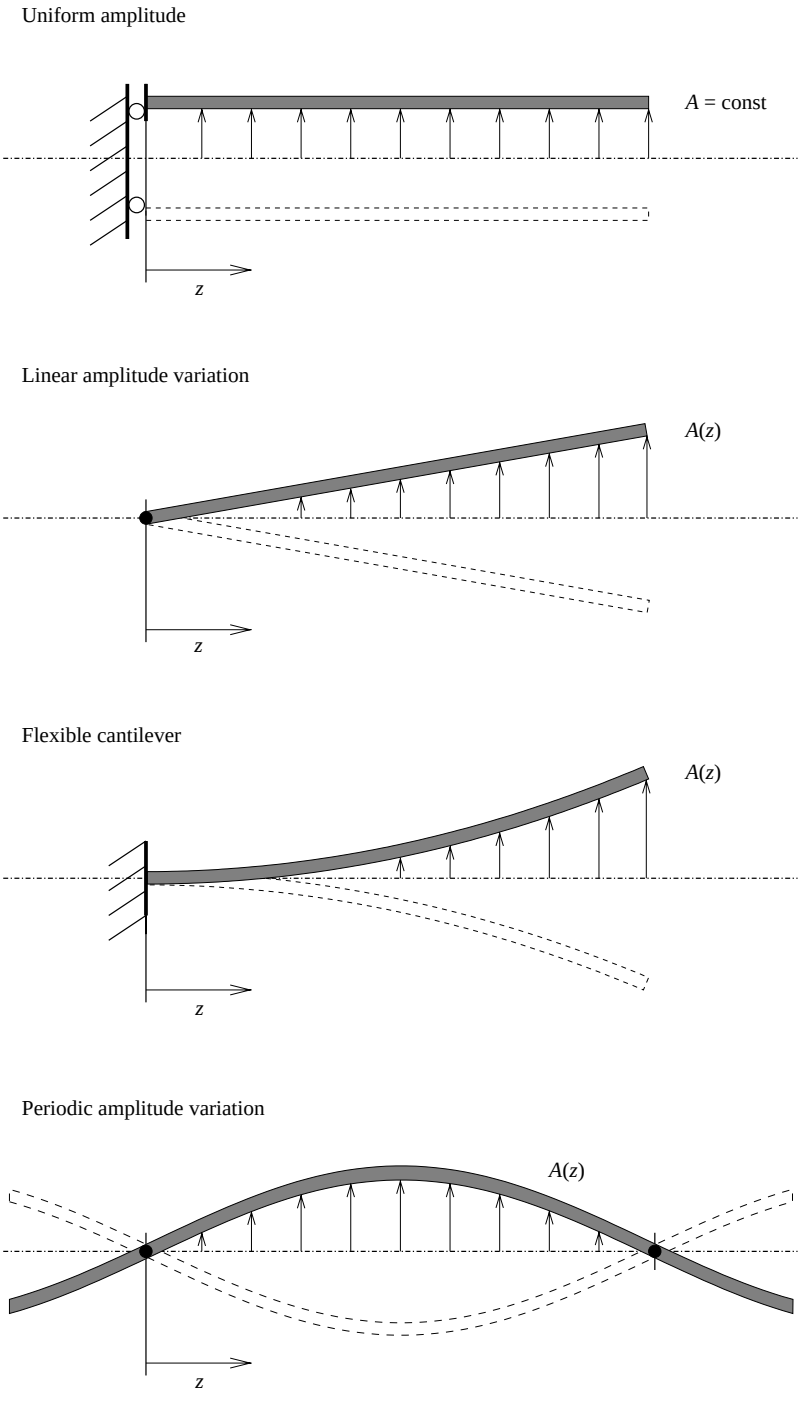

FIGURE 1. Different types of spanwise amplitude distributions investigated in vortex-induced vibration studies of cylindrical bluff bodies.

As stated above, one is interested in using the quasi-uniform approximation to predict dynamics, using force coefficients input from uniform-cylinder data (as done for example in offshore design codes using the classical 'Morison's' equation in wave

Inertia ratio	I^*	I/I_d
Mass ratio	m^*	m/m_d
Structural damping coefficient	ζ	$c/2\sqrt{k(I+I_A)}$
Normalized velocity	U^*	$U/f_N D$
Normalized tip amplitude	A^*	A/D
Frequency ratio	f^*	f/f_N
Reynolds number	Re	$\rho U D/\mu$
Strouhal number	S	$f_V D/U$

TABLE 1. Definition of the relevant non-dimensional groups. In these groups, f denotes the oscillation frequency, while f_N is the natural frequency of the system in water. The vortex shedding frequency of a stationary cylinder is f_V. The added moment of inertia I_A is given by $I_A = C_A I_d$, where I_d is the inertia of the displaced fluid with respect to the pivot point and C_A is the potential added-mass coefficient ($C_A = 1$ for circular cylinders). A^* and f^* have subscripts which refer to the X- and Y-direction. However, for simplicity, we choose to use f^* in several places in the paper to mean the transverse frequency f_Y^*. Furthermore, $m =$ mass per unit length, $m_d =$ displaced fluid mass per unit length, $D =$ cylinder diameter, $U =$ free-stream velocity, $\rho =$ fluid density and $\mu =$ viscosity.

flows). In the case of negligible streamwise motion, this would be a possibility with this problem, but in the presence of significant streamwise motion, the required force coefficient data set would be prohibitively large, as it would depend on several different parameters (the amplitudes in the X- and Y-directions, the phase between these motions and the normalized frequency, etc.). In that case, the approach of specifically chosen experiments and numerical simulations would be useful guides. The present type of study also contributes to determining the regimes where such predictive vortex and structure dynamics would be reasonable and where they would not.

This experiment comprises a cylinder which is pivoted at the top end using a thin flexible (coaxial) pin, enabling vibrations as a pendulum in X- or Y-directions, parallel or normal (respectively) to the flow direction in the Cornell-ONR Water Channel. The oscillating mass and natural frequencies are thus equal in the X- and Y-directions, and this case is therefore related to our recent study on a cylinder in uniform-amplitude vibrations, which is a case in which there are identical mass and frequencies in X- and Y-directions (Jauvtis & Williamson (2003, 2004*a*, *b*).

We introduce here a set of non-dimensional parameters that define the present experiments. The pivoted cylinder has, associated with it, a natural frequency in water (f_N), a moment of inertia about the pivot point (I), structural damping (c) and the spring stiffness from the coaxial pin (k), which is situated at the top of the vertical cylinder, just above the free surface of the flowing fluid in our water channel. These parameters, and the cylinder dimensions, lead to the non-dimensional groups in table 1. The inertia ratio I^* is almost identical to the mass ratio m^* for the uniform cylinder case, since the mass is uniformly distributed along the span. Also, the inertia ratio, $I^* > 1$ in the present experiments, otherwise the body starts to float, which is a problem, since our pivot is at the top.

For the case of uniform-amplitude vibration, there are a large number of studies, as mentioned earlier. For Y-motion, one expects a resonance when the speed of the flow is such that the vortex frequency for the non-oscillating body (f_V) is near to the structural natural frequency (f_N), which will occur when $U^* = U/f_N D \sim U/f_V D = 1/S$, where S is the Strouhal number. With a Strouhal number of around 0.2, one expects resonant oscillations near a velocity, $U^* \sim 5$. The work of Feng (1968) at high mass

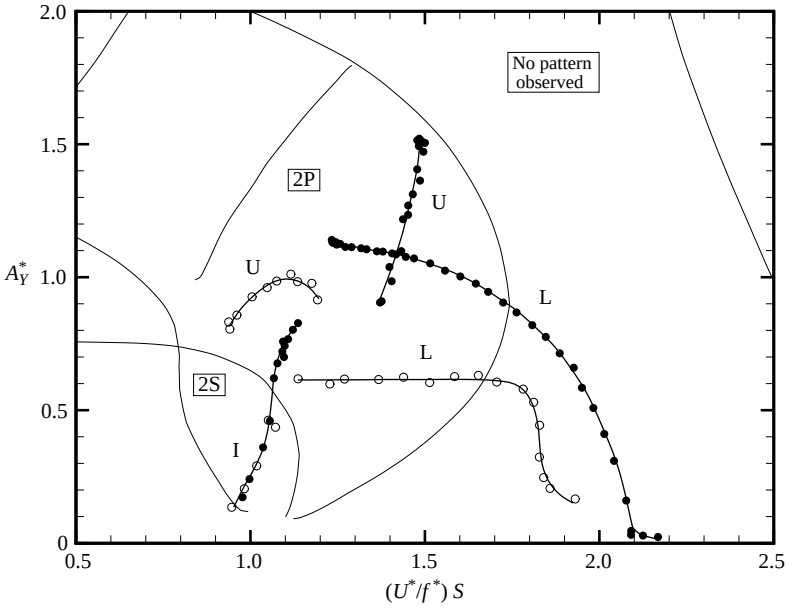

FIGURE 2. Transverse oscillation amplitude A_Y^* versus the 'true' reduced velocity $(U^*/f^*)S$ for the pivoted cylinder (●), $I^* = 1.03$ and an elastically mounted rigid cylinder (○), $m^* = 1.19$ by Govardhan & Williamson (2000) plotted on the map of vortex modes (Williamson & Roshko 1988). Both cases show three distinctly different branches, namely the initial branch (I), the upper branch (U) and the lower branch (L).

ratios, $m^* = 320$, demonstrated that the resonance of a body will occur over a regime of normalized velocity U^* such that $U^* \sim 5$ to 8. Two response amplitude branches are found, which are shown by Brika & Laneville (1993) and by Govardhan & Williamson (2000) to be due to two modes of vortex formation, as follows. For the 'initial' branch of response, the vortex wake comprises a '2S' mode, representing two single vortices formed per cycle. The 'lower' branch comprises the '2P' mode, whereby two vortex pairs are formed per cycle (as originally defined in Williamson & Roshko 1988 from their forced vibration study). However, at low mass and damping (m^* typically of the order 5 to 10), and higher amplitudes of response, three response branches are found to exist (Khalak & Williamson 1996, 1999; Govardhan & Williamson 2000), namely the 'Initial' branch (with a 2S vortex wake mode), the 'Lower' branch (with a 2P mode), and a further distinctly higher-amplitude mode appearing between these two other branches, namely the 'upper' branch (also with a 2P mode of vortex formation). Typical initial (I), upper (U) and lower (L) response branches can be seen, in figure 2, for the uniform vibration case of Govardhan & Williamson (2000), where these branches are defined by the open symbols.

A good correspondence has been found (Brika & Laneville 1993; Khalak & Williamson 1999; Govardhan & Williamson 2000) between the visualized or measured vortex wake modes (using digital particle image velocimetry (DPIV)) for the free vibration response branches, and the Williamson & Roshko (1988) map of vortex modes defined in the plane of amplitude (A_Y^* = transverse amplitude/diameter) and velocity (U^*), which was compiled from controlled (or forced) vibration experiments. We shall use this map of modes as the basis for comparison of response branches in the present study also. The initial branch lies in the 2S mode regime, while the upper

and lower branches lie comfortably in the 2P mode regime, as one might expect. In this figure, we renormalize the velocity axis as follows. For given mass and damping, the response amplitude will be a function of its actual transverse oscillation frequency (f) relative to the frequency of vortex shedding in the absence of vibration (f_V). We therefore employ a normalized velocity $(U^*/f^*)S$, which is equal to (f_V/f), and which has previously yielded a good collapse of amplitude data for a set of response plots (made at different mass ratios), in Khalak & Williamson (1999).

The modes and responses discussed above are found for strictly transverse vibration in a fluid flow. However, in recent studies Jauvtis & Williamson (2003, 2004*a*, *b*) investigated to what extent these transverse response modes and amplitudes are influenced by the body's freedom to respond in the streamwise direction. In almost all practical cases, cylindrical structures (such as riser tubes or heat exchangers) have the same mass ratio and the same natural frequency in both the streamwise (X) and transverse (Y) directions. Two recent arrangements that ensure such conditions are the air bearing platform of Don Rockwell's group at Lehigh University (private communication, 2004), and the pendulum setup in the present paper. These studies demonstrate a set of response branches, in contrast to previous XY experiments (see Moe & Wu 1990; Sarpkaya 1995). Even down to the low mass ratios, where $m^* = 6$, it is remarkable that the freedom to oscillate in-line with the flow hardly affects the response branches, the forces, and the vortex wake modes. These results are significant because they indicate that the extensive understanding of vortex-induced vibration for Y-only body motions, formulated for 3–4 decades, remain relevant to the case of two degrees of freedom. However, there is a marked change in the fluid–structure interactions when mass ratios are reduced below $m^* = 6$. A new response branch with significant streamwise motion appears in what Jauvtis & Williamson (2004*a*) defined as the 'super-upper' branch, which yields massive amplitudes of three diameters peak-to-peak ($A_Y^* \sim 1.5$). This response corresponds to a new periodic vortex wake mode, which comprises a triplet of vortices being formed in each half-cycle, defined as a '2T' mode following the terminology that Williamson & Roshko (1988) introduced.

The dynamics of the body are dependent on the fluid forcing (and thereby the vortex dynamics) along the span, and it is of interest to determine to what extent the vortex modes (and spanwise distribution of fluid forcing) might be predicted, based on uniform-amplitude results, i.e. based on the quasi-uniform assumption described earlier. One might question whether particular wake modes persist along the complete span, or whether two modes of vortex formation exist along different spanwise regimes. Such a phenomenon has been discovered in the case where a tapered body is forced to vibrate normal to a flow (Techet *et al.* 1998), and has become known as the Hybrid mode comprising 2S and 2P modes coexisting along different portions of the span. At the boundaries between these cells of different vortex modes are situated 'vortex dislocations', where the vortices split into two parts (Williamson 1989, 1992; Eisenlohr & Eckelmann 1989). We might naturally expect to see such phenomena in the present case. Lucor *et al.* (2001), in the group of George Karniadakis at Brown, also observe structures near the nodes of their vibrating cable to be vortex dislocations. The existence of such vorticity dynamics is important to the distribution of fluid loading along the span, and therefore to the vortex-induced vibration of a flexible body.

We shall distinguish between the transversely vibrating tapered cylinder of Techet *et al.* (1998), and our pivoted cylinder case, noting again that both of these have a linear spanwise variation of normalized amplitude. We plot such a variation of

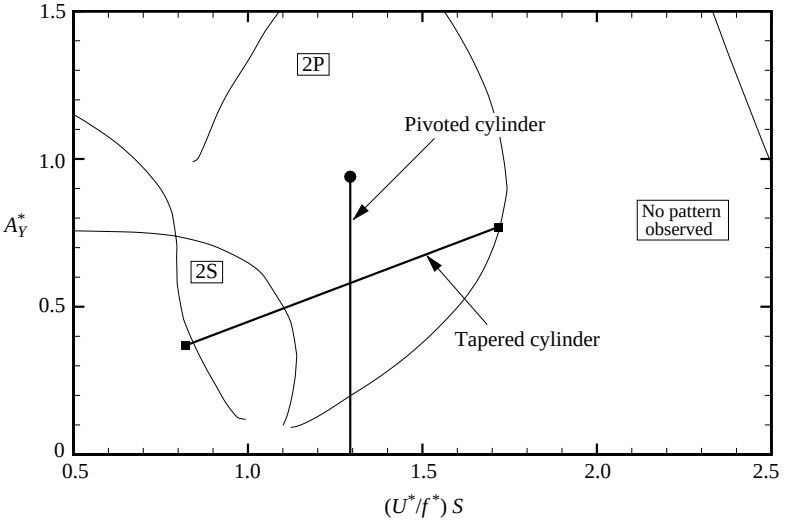

FIGURE 3. Amplitude distributions along the span of the pivoted cylinder (●) used in this study and the tapered cylinder (■) of Techet *et al.* (1998) plotted on the map of vortex formation modes.

amplitude along the span (A_Y^*) versus $(U^*/f^*)S$ in figure 3, over the Williamson & Roshko (1988) map of vortex modes. For the tapered cylinder, the black squares denote the ends of the cylinder, with the thinner tapered end to the right. One can see that the span of the cylinder crosses through the 2S and 2P mode regimes, suggesting interesting vortex dynamics along the span, and as noted above, the experiments yield the 2S-2P hybrid mode. Our own case of the pivoted cylinder is represented by the vertical line in figure 3, where the precise value of $(U^*/f^*)S$ depends on flow speed and vibration frequency in a given set-up. It is clear that we might expect such a 2S-2P hybrid mode in our system also, if $(U^*/f^*)S$ is in the vicinity of 1.0. However, we shall also find that the ability of our system to vibrate streamwise will admit further modes.

Van Voorhees & Wei (2002) have studied the response and wake modes found at the centre span of a pivoted cylinder, where the vibrations are confined to transverse motion. They report modes which have a similarity to those found for the uniform-amplitude cylinder, and they investigated the existence of spanwise flows along the vortex cores, with extensive PIV studies. Also of relevance to the present paper is the study by Fujarra *et al.* (2001), where a flexible cantilever exhibits response branches which appear to be an initial and lower branch, and a reasonable agreement with responses from the uniform-amplitude vibration case, at comparable mass and damping, is shown.

It is significant to note that full-scale piles in an ocean current (Wooton *et al.* 1972), and similar cantilever models in the laboratory (King 1974), have been found to vibrate. The measured vortex-induced vibrations involved significant streamwise motion, although the peak amplitudes of the cantilever tip ($A_X^* \sim 0.15$) are less than typically found for resonant transverse vibration of very light structures ($A_Y^* \sim 1.0$). As reviewed by Bearman (1984), and by Naudascher (1987), these streamwise vibrations are due to the fact that, as each vortex is shed, a fluctuating drag is generated, so that the in-line forcing frequency (f_X) is twice that for the transverse

direction (f_Y). The forcing induces the body to vibrate in-line with the flow, if the normalized velocity is close to $U^* \sim 1/2S$ (at which point, $f_X \sim f_N$), and King (1974) showed that the wake formation in this case comprised a classical vortex street (antisymmetric) pattern. Interestingly, these investigators also discovered a second mode of streamwise vibration, when the wake formed symmetric vortex pairs close to the body. Both modes have been found by vibrating a cylinder (with uniform amplitude) in-line with the flow (Griffin & Ramberg 1976; Ongoren & Rockwell 1988). Ongoren & Rockwell presented very clearly the various modes as the forcing frequency of the body was varied. In our case here, we are primarily interested in the transverse vibration modes, and judging by the work of Jauvtis & Williamson (2004*b*), our very slight streamwise motion in the regime $U^* \sim 2.5{-}5$ is perhaps related to the fact that the mass ratio m^* (or I^* in this case) is not sufficiently small to yield a distinct resonance in this regime, although this is not clear.

Despite the fundamental differences between a pivoted body, with linear amplitude gradient, and the uniform-amplitude case, there are some basic similarities in vibration response, as we see in figure 2, shown earlier. Both systems exhibit an initial branch (I), an upper branch (U), and a lower branch (L), in the case of similar very low inertia and mass ratios ($I^* = 1.03$ versus $m^* = 1.19$) and small mass–damping ratios (which are significant to the peak amplitude found in the system response) having values: $I^*\zeta = 0.0023$ versus $m^*\zeta = 0.0060$ where ζ is the damping ratio defined in table 1 and in Appendix B. However, the maximum amplitudes are very different (noting also that A_Y^* for the pivoted body measures the tip amplitude), and the shape and location of the upper branch is remarkably different for each system. The pivoted body exhibits two response branches, which cross over each other, which is an unusual phenomenon. We set out in this paper to explore further these structural dynamics, and also to study the vortex dynamics giving rise to such body motions.

Finally, as a part of this introduction, we briefly look at the influence of the mass (or inertia) of the structure on the response, in figure 4. The synchronization regime (the extent of U^* over which there is significant response amplitude) increases markedly as inertia decreases (as found when m^* decreases in Griffin & Ramberg 1982 and in Khalak & Williamson 1999). However, there is a reasonable collapse of the three different sets of data, when plotted against the 'true' reduced velocity $(U^*/f^*)S$ in figure 4. The differences in maximum amplitudes are partly attributed to differences in the product $I^*\zeta$ (inertia–damping), which influence the peak amplitudes, analogously to the uniform-amplitude case. For high inertia–damping (or high $I^*\zeta$), we observe only two response branches (initial and lower branches), while at sufficiently small ($I^*\zeta$), in the case of the plastic cylinder, we find three branches (initial, upper and lower). This scenario is directly analogous to the character of the response for the uniform-amplitude case (Khalak & Williamson 1996, 1999). We shall choose the lightest body as the principal case in this work, as it exhibits the most interesting dynamics and vortex modes.

In the following section, we discuss briefly the experimental approach and arrangement, followed by the modes of vortex-induced vibration in § 3. One of the most interesting and revealing phenomena is the fact that two of the response branches cross over each other in the response plot. The explanation of this will involve an understanding of the key influence of streamwise motion, and we develop a three-dimensional plot that is an extension of the Williamson & Roshko (1988) map of modes, demonstrating that the response branches exist in different parameter space. New vortex dynamics modes associated with these response branches are shown using digital particle image velocimetry (DPIV) in § 4. We derive simple equations of

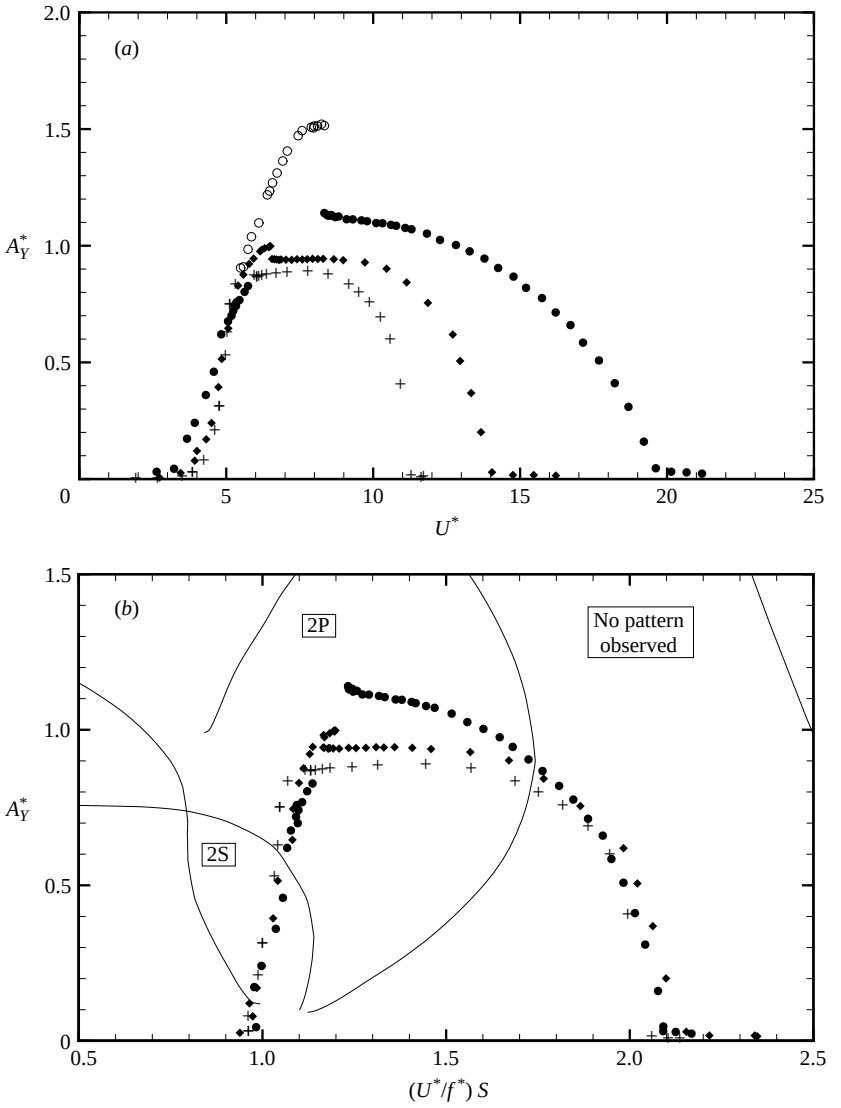

FIGURE 4. Transverse oscillation amplitude A_Y^* for three pivoted cylinders of different inertia, showing a good collapse of data when plotted versus the 'true' reduced velocity $(U^*/f^*)/S$ instead of only U^*. The open symbols correspond to the upper branch for the plastic cylinder. In (*b*); the upper branch for the lightest body has been left out, for clarity. ●, ○, plastic – $I^* = 1.03$; ◆, aluminium – $I^* = 2.68$; +, steel – $I^* = 7.69$. At the peak amplitude, $Re \sim 1000$ (for $I^* = 1.03$); $Re \sim 1360$ (for $I^* = 2.68$); $Re \sim 1300$ (for $I^* = 7.69$).

motion (in the X- and Y-directions) for the pivoted body in § 5, which will reveal a critical inertia (or mass) below which our pivoted body can vibrate at large amplitude up to infinite normalized velocities, in direct analogy with such critical masses found for the uniform-amplitude case in Govardhan & Williamson (2000, 2002), and for the XY motion of a cylinder in Jauvtis & Williamson (2004*b*), and also in the case of the vortex-induced vibrations of a sphere in Govardhan & Williamson (2005). The conclusions are presented in § 6.

2. Experimental details

The present experiments were conducted in the Cornell-ONR Water Channel facility. Khalak & Williamson (1996) provide details concerning this water channel facility, whose Lucite test section is 38.1 cm wide, with a water depth of 46 cm, and with a length of 250 cm. The cylinder was arranged such that the bottom tip oscillated with a 2 mm clearance from a horizontal end plate surface. The motion of the illuminated tip was recorded in the X- and Y-direction at a rate of 100 samples per second by an optical bi-axial displacement transducer, mounted underneath the water channel. The top end of the cylinder (see figure 5) comprised a thin coaxial pin attached securely to the central axis of the cylinder, and also fully fixed at a point just above the free surface. The natural frequency was adjusted by changing the diameter of the spring steel pin as well as its length. The system is equivalent to a pivot point with an attached axisymmetric torsion spring, and yields an axisymmetric pendulum, as long as the pin is much shorter than the cylinder, which was the case in all experiments ($l_{pin}/L \ll 1$).

This pivot system allowed axisymmetry and thereby an equal inertia and natural frequency in the X- and Y-directions. The coordinate Z measures distance vertically downwards from the water surface. Our cylinders have diameters of 9.6 mm and 12.8 mm, with length–diameter ratios (L/D) of 41 and 31 respectively. Three principal cases are investigated, namely a plastic cylinder (density $\rho = 1.03\,\mathrm{g/cm^{-3}}$) as the 'light' case, an aluminium one ($\rho = 2.68\,\mathrm{g/cm^{-3}}$) as the 'medium' case, and a steel one ($\rho = 7.69\,\mathrm{g/cm^{-3}}$) as the 'heavy' body. Over all the present experiments, the maximum angular deflection (α) of the cylinder, relative to the vertical, amounts to 4°(for the lightest cylinder).

DPIV was used to determine the vorticity in various planes along the submerged cylinder length, and the implementation of this technique is described in detail in Govardhan & Williamson (2000). In all presented colour contour plots of vorticity in this paper, the blue colour represents clockwise vorticity, while the red is anticlockwise vorticity. Since it was important to capture vorticity structures along the span, the DPIV measurements were performed at seven equally distributed spanwise positions (cross-sections A to G), as indicated in figure 5. This was done for all flow speeds. Each DPIV run comprises 40 s of data, capturing 50 to 70 cycles of cylinder oscillation. We employ phase averaging in this study, averaged over 10 consecutive cycles in the centre of each dataset, to extract the principal spanwise (z) component of vorticity for each cross-section.

3. Vortex-induced vibration of the body

We shall present, in this section, the characteristics of the response of the pivoted cylinder for the very light body (of plastic), with a small inertia $I^* = 1.03$ (equivalent to $m^* = 1.03$). In these experiments, the Reynolds number at maximum amplitude ($U^* \sim 9$), is $Re \sim 1000$.

3.1. *Classical response of the body*

We show the transverse and streamwise amplitude, and response frequency, versus normalized velocity U^*, in figure 6. The amplitudes here are averages evaluated over the complete time traces recorded in the experiments. If one were to look only at the plot of transverse amplitude (A_Y^*) it would appear that there are only two response branches, namely an initial and lower branch. However, there is a very slight discontinuity if one looks closely at the response for $U^* \sim 5.5$, and it

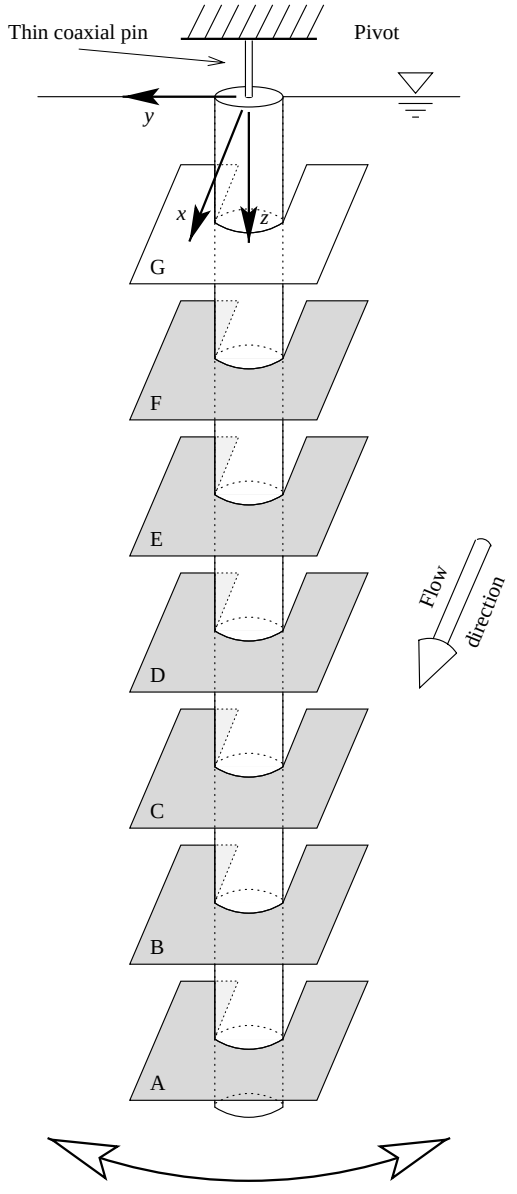

FIGURE 5. Setup and labelling of the DPIV layers (A, B, C, ...) along the span of the pivoted cylinder.

is only by observing the obvious large jump in streamwise amplitude A_X^* that one deduces that both an initial and upper response branch exists. (This difficulty in determining whether an upper branch exists was evident in the cantilever studies of Fujarra *et al.* 2001. One has to look at other data, in this case the streamwise motion, to provide evidence for mode changes. In other cases, the phase of the fluid force is an excellent indicator, in order to evaluate whether a distinct upper branch is present.) The upper branch here corresponds to a large transverse amplitude, rising

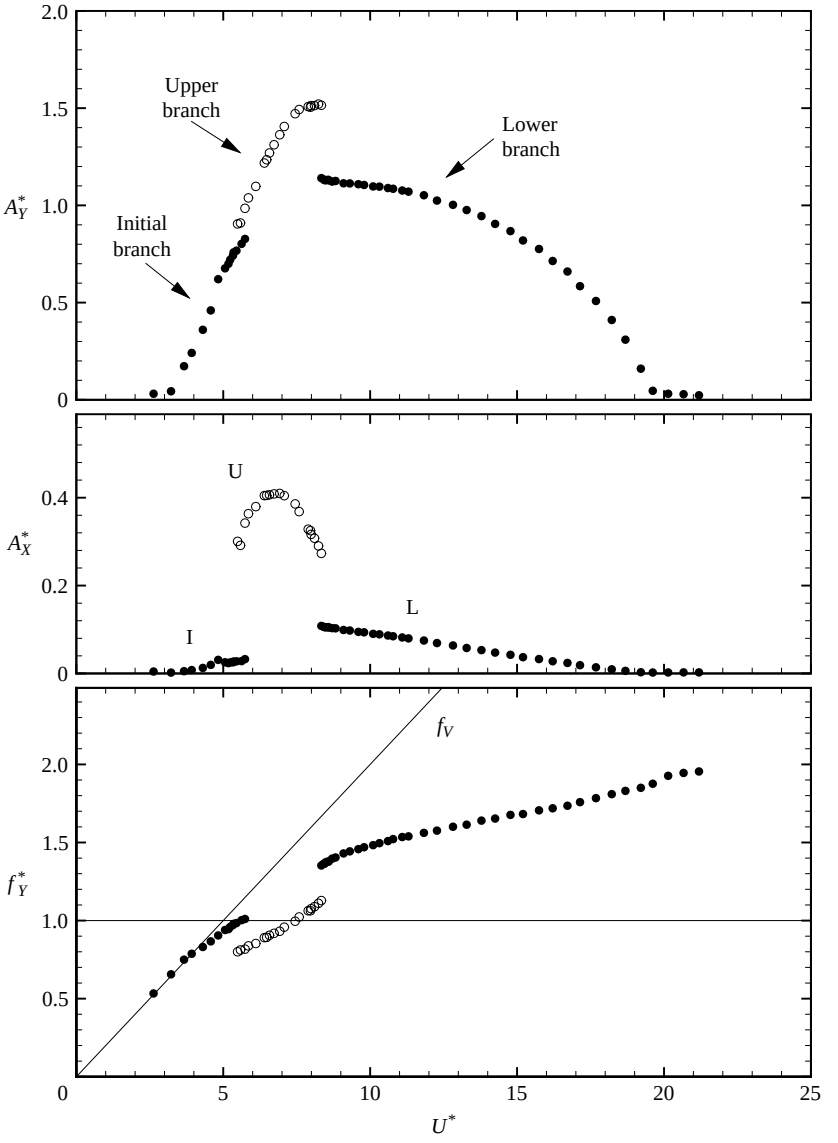

FIGURE 6. Transverse and streamwise amplitude (A_Y^*, A_X^*) as well as frequency f_Y^* versus reduced velocity U^* for the plastic cylinder, showing a distinct separation of the three response branches. The open symbols separate the upper branch from the initial and lower branch.

to $A_Y^* \sim 1.5$, and a significant streamwise amplitude A_X^*, which is roughly 30% of A_Y^*. As stated earlier, there is very little streamwise motion at low $U^* \sim 2.5-4$, in these particular experiments, where one might expect the in-line vibration modes found for the piles and cantilevers of Wooton *et al.* (1972) and King (1974). Possibly a reduction in inertia of the body would realize these modes.

The transverse frequency f_Y^* is also presented in figure 6, and we have omitted the streamwise frequency, f_X^*, since it is precisely twice f_Y^*, throughout the regimes of response. The frequencies, for the first part of the initial branch, which corresponds to very small amplitudes, align with the Strouhal frequency (f_V) for a stationary cylinder at comparable Reynolds numbers. As we increase U^* in the initial branch,

the frequency f_Y^* diverges from f_V, until it reaches the natural frequency in water ($f^* = f/f_N = 1$). At this point the frequency drops down by $\Delta f^* = -0.17$ to the lower frequency of the upper branch. It then continues to increase with U^* in the upper branch. This jump will become very important in the later discussion of the dynamics, in § 3.2. The end of the upper branch is clearly marked by another jump of $\Delta f^* = +0.24$, to the higher frequency of the lower branch. The frequency continues to increase with velocity along the lower branch, until the cylinder desynchronizes around $U^* \sim 19$. At this point, the principal energy in the displacement spectrum is again found at the Strouhal frequency (not visible in figure 6), with some energy retained at the frequencies around $f^* = 2.0$. In the uniform-amplitude case, the lower branch exhibits a roughly constant response amplitude (and an almost constant frequency f^*) whereas for the pivoted case, the amplitude gradually diminishes until desynchronization.

We compute a phase θ between the vibrations in the X- and Y-directions in figure 7, as a function of velocity U^*. We also show Lissajous figures for trajectories of average cycles for five distinct values of U^* within the response plot, in the initial branch, in the upper branch, and in the lower branch. It is again evident that the largest streamwise vibrations occur in the upper branch, similar to the Lissajous figures for the upper branch in the case of XY-motion of a cylinder (Jauvtis & Williamson 2004*b*). The first and last Lissajous of the lower group denotes the start and end point of the upper branch. Given the marked difference in the character of the body XY dynamics for the three branches, we might expect quite different vortex wake modes leading to such dynamics, and this will indeed be shown later in § 4.

3.2. *The crossover point*

If the amplitude response is presented as a function of the 'true' reduced velocity $(U^*/f^*)S$, as in figure 8, we observe a remarkable effect where the upper and lower response branches cross over each other, and this is marked by the bull's eye (where $A_Y^* = 1.08$; $(U^*/f^*)S = 1.42$). The crossover is caused by the fact that the frequency jumps by $\Delta f^* = +0.24$ up to a higher value, when the amplitude drops from the upper to lower branch. This tends to shift the lower branch to the left when amplitude is plotted versus $(U^*/f^*)S$. For reference, we can see, as one might expect, that this crossover point actually represents two points in the lower response diagram, where amplitude is plotted versus normalized velocity U^* (with quite dissimilar values of $U^* = 6.0$ and 11.0). Prior to further discussion below, we may note that not only are the vibrations near the crossover point close to sinusoidal, but the transverse-vibration time traces are almost identical for the upper and lower branch cases.

The cylinder tip response, in figure 8, is plotted over the Williamson & Roshko (1988) map of vortex wake modes, for uniform-amplitude cylinders in transverse vibration. Considering the predicted patterns of vortex formation from this map, the following question arises: since the relative path of the body through the fluid is supposedly the same for each branch where they cross over each other (the bull's eye) then should we find the same vortex wake modes along the span for each response branch? (In this case, one might suppose that the 2P wake mode will appear over much of the span, based on the Williamson-Roshko map.) In reality, there must of course be a difference between the two cases. This difference is the streamwise amplitude of oscillation A_X^*. The upper branch has a value of A_X^* that is far larger than found in the lower branch, as can readily be seen in figure 6. We must therefore define a new three-dimensional plot, in figure 9, where the streamwise amplitude A_X^* is measured by the vertical distance above the classical plot of A_Y^* versus $(U^*/f^*)S$. Now

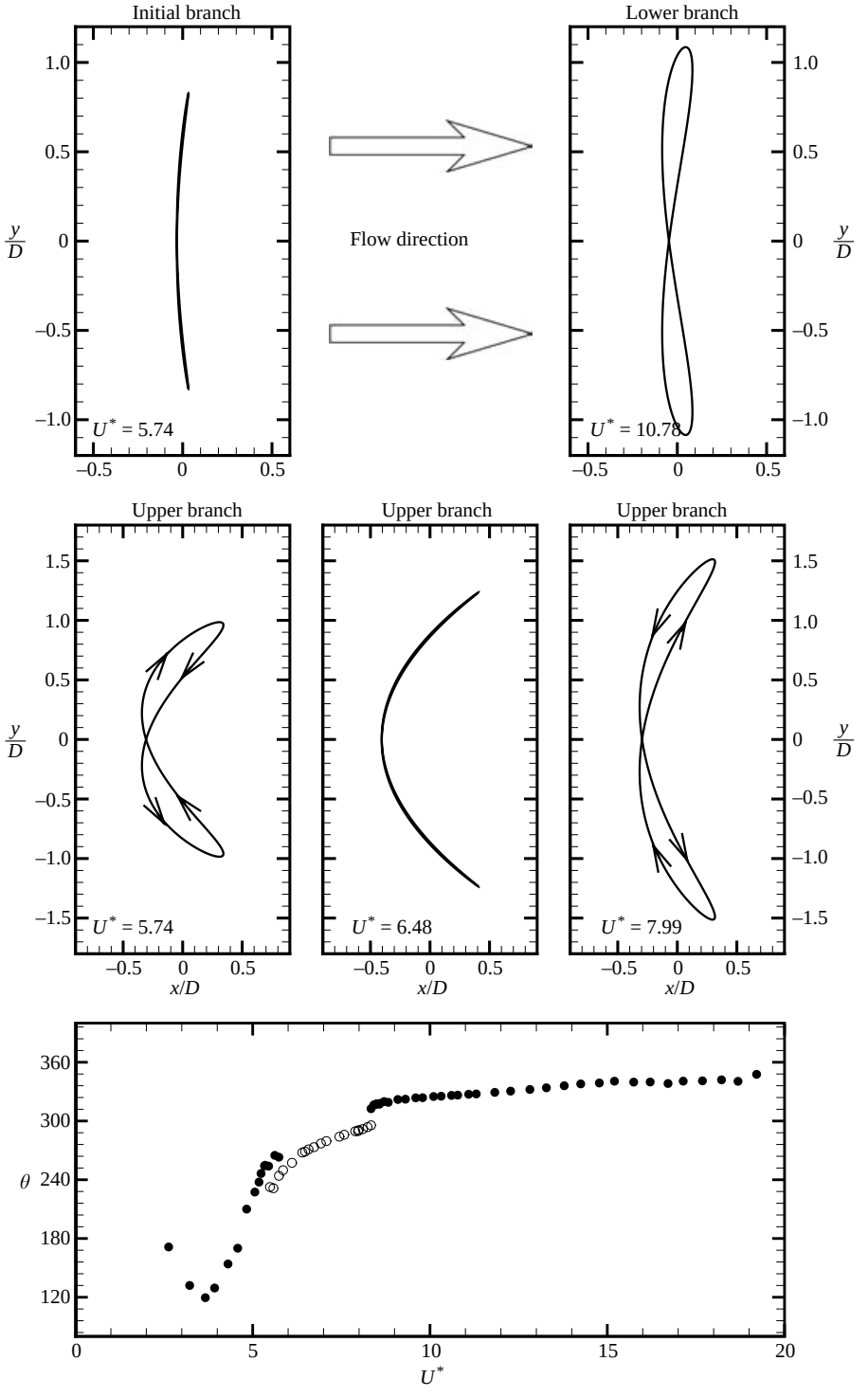

FIGURE 7. Phase θ between the transverse and streamwise motion of the cylinder as a function of non-dimensional velocity U^*. The Lissajous figures show characteristic average motions of the cylinder in the $(x/D, y/D)$-plane for the initial, upper and lower branch. The Lissajous for the initial branch and the first Lissajous of the upper branch occur at the same $U^* = 5.74$.

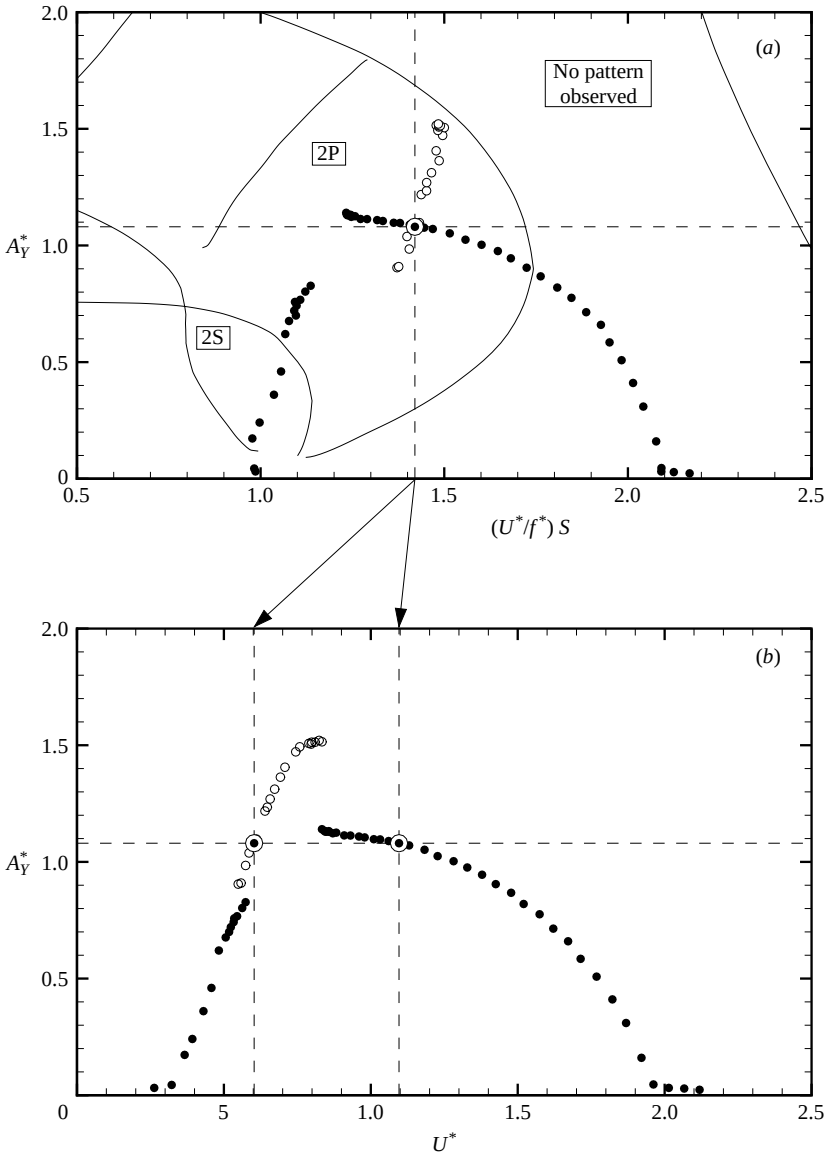

FIGURE 8. (*a*) Transverse amplitude A_Y^* as a function of the 'true' reduced velocity $(U^*/f^*)S$ showing a crossover point (⊙) between the upper and lower branch. However, this point actually corresponds to two different positions within the classical amplitude response plot given in (*b*).

we see very clearly that the (red) upper branch response 'flies' well above the (blue) lower branch, and is in a markedly different parameter space. This representation of the data also shows neatly that the crossover point denoted again by the bull's eye symbols will only exist in the projection onto the bottom plane, as in figure 8. We might therefore expect to see different vortex wake modes for each branch, and this will be explored in § 4.

Finally, it is of interest to study the different kinds of jump phenomena between the different response branches. As shown schematically in figure 10, we find a

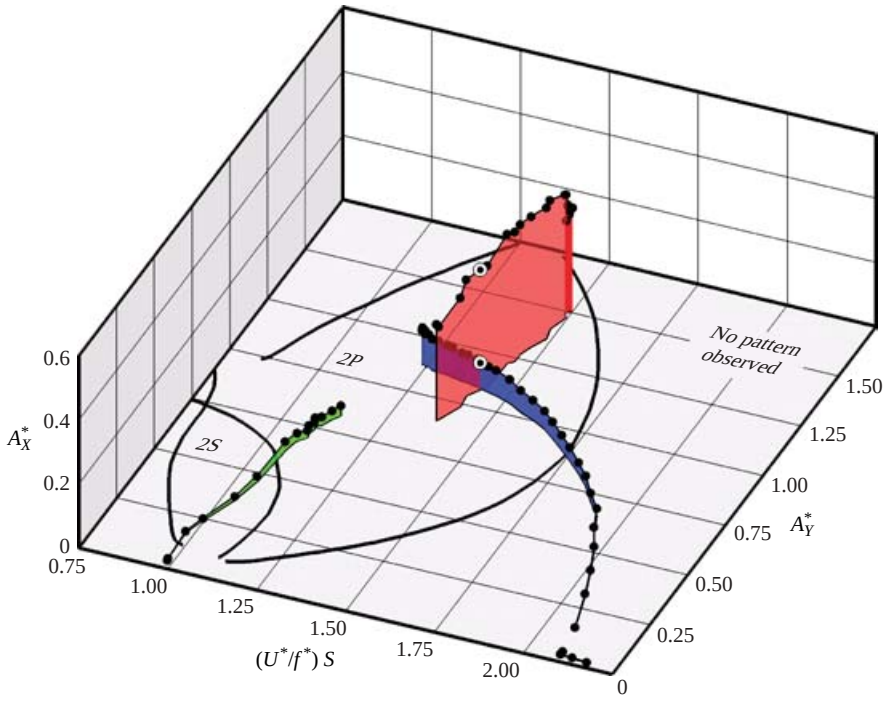

FIGURE 9. Three-dimensional response plot, showing the transverse amplitude A_Y^* and the streamwise amplitude A_X^* as a function of $(U^*/f^*)S$. The crossover point is again denoted by a bullseye symbol (⊙), clarifying that the two points only align in the projection of the cylinder response in the $((U^*/f^*)S, A_Y^*)$-plane. The map of vortex modes is shown in the two-dimensional bottom plane.

hysteretic jump between the initial and upper branches, and an intermittent switching between the upper and lower branches. To avoid confusion in the diagram, the solid arrows denote the direction followed along the amplitude solutions when velocity (U^*) is increased. The intermittent switching is illustrated well by the displacement and frequency as a function of time, in figure 10(*b*). The system seems to stay for long periods of time at one or the other branch (points A or B in the amplitude plot), but to change rather abruptly between them in an intermittent fashion. The instantaneous frequency is determined by the use of the Hilbert Transform, whose use in these vortex-induced vibration problems was exploited (and discussed) in Khalak & Williamson (1997); Khalak & Williamson (1999). One notes that the periods of higher amplitude of the upper branch correspond to the lower frequency levels, which is consistent with the response plots in figure 6.

4. Vortex formation modes

There are three distinct response branches when the pivoted cylinder is light, or has a small value of $I^*\zeta$. We study, in this section, the vortex wake modes which give rise to these body dynamics, in particular for the plastic cylinder ($I^* = 1.03$), although similar vortex dynamics were observed for the response branches of the aluminium body ($I^* = 2.68$). The Reynolds numbers for the plastic cylinder, where we observe such three-dimensional vortex modes as exhibited in this section, and in Appendix A, are as follows: 2S mode ($Re \approx 700$); 2P mode ($Re \approx 1600$); 2S-2P hybrid mode

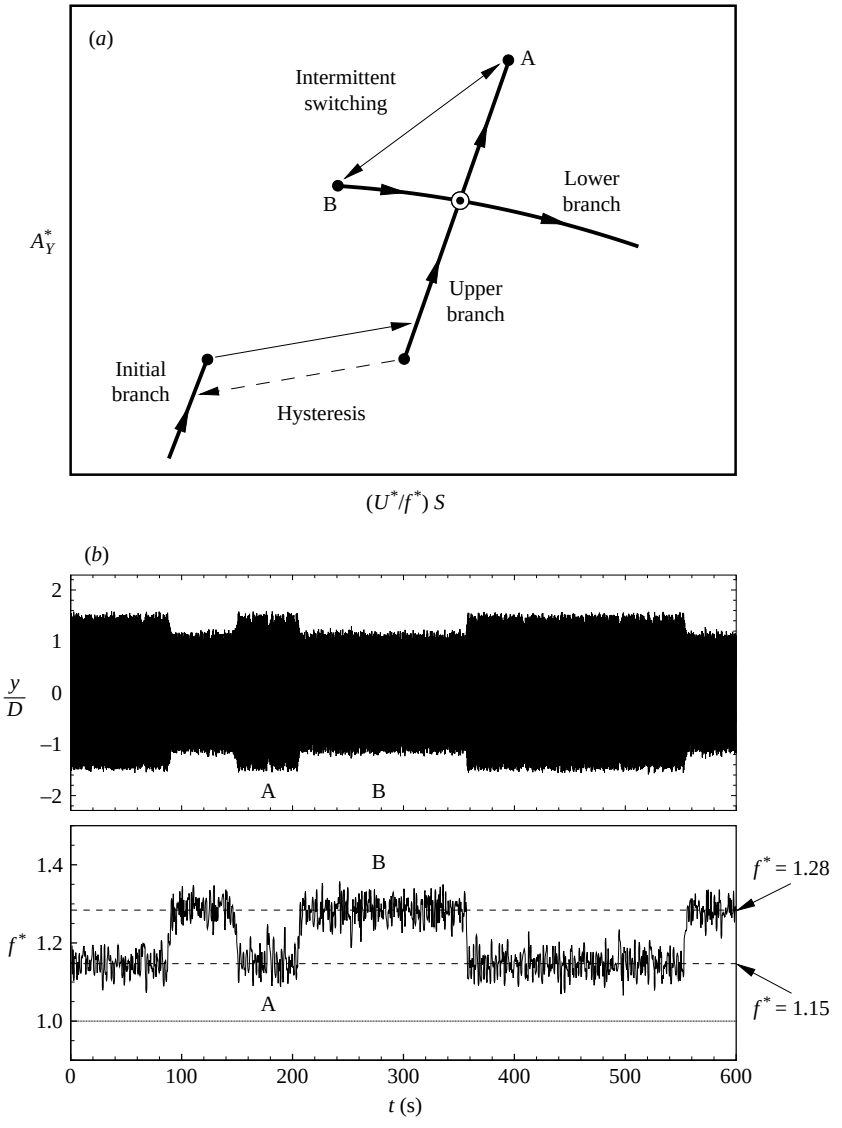

FIGURE 10. (*a*) The different jump phenomena between the initial, upper and lower branches. The solid arrows correspond to increasing free-stream velocity and the dashed arrow to decreasing velocity. In (*b*), the transverse position y/D and instantaneous frequency of transverse oscillation f^*, evaluated by the use of Hilbert Transform was acquired over a period of 600 s showing the intermittent switching very clearly.

($Re \approx 1100$); 2C mode ($Re \approx 1200$). It should be noted that in this section the pivot is situated at the bottom of the figures, whereas in the physical experiment, the pivot is at the top. With the pivoting cylinder arrangement in this paper, we are not in a position to closely relate vorticity dynamics to the local (spanwise) fluid force on the body.

4.1. *Vortex dynamics with small streamwise oscillations*

In this section, we shall study the vortex dynamics associated with the body when there are only small streamwise vibrations, so that we will look at the modes throughout the initial and lower branches. One of the questions one might ask is: to what extent

can one predict the vortex wake modes based on the Williamson & Roshko (1988) map of modes? Use of this map would require a 'quasi-uniform' assumption, whereby one supposes that locally at some spanwise position, the predicted vortex wake mode is given from the map of modes, using data for uniform-amplitude conditions. Considering first the initial branch (see figure 9), we can see that it has a portion within the 2S mode regime of the Williamson–Roshko map of modes, and a portion where the tip of the body would be in the 2P mode. In the latter case, we may expect that some of the body nearer the pivot would retain the 2S mode, suggesting the possible existence of a 2S-2P hybrid mode. We can further predict that where the tip amplitude runs along the lower branch, the wake mode would be 2P along the whole span. We shall go on to exhibit these different three–dimensional modes, in agreement with predictions from the map of modes.

For brevity in this presentation, we have placed the less complex modes in Appendix A, as the 2S and 2P mode are well-known for the uniform-amplitude case. Evidence for these modes in the case of the pivoted cylinder is nevertheless documented in this Appendix. In essence, the 2S mode along the span is indeed found in the initial branch, and an example is shown in figure 19, for $U^* = 4.0$. The cross-sectional planes, at which spanwise vorticity is measured, correspond to the planes described in figure 5. This 2S mode is predicted for tip amplitudes below the 2S-2P boundary in the map of modes (see figure 9). On the other hand, when the tip amplitude lies along the lower branch, we find a clear 2P mode throughout the span, as shown in figure 20. In fact, the vorticity dynamics for these two modes for the pivoted cylinder compare qualitatively very well with modes found for uniform-amplitude cylinders, as demonstrated in figure 21, where a comparison is made with vorticity distributions of Govardhan & Williamson (2000) for the 2S and 2P modes. In both types of problem, the phase of the vortex formation in the near wake shows a jump of around 180°, when the system passes between the 2S and the 2P modes.

If we now look at the wake flow using dye visualization in figure 11, for a case where the tip amplitude extends into the 2P mode regime of the initial branch, the vortex mode does indeed depend on the spanwise location at which the dye is introduced. One sees the appearance of a 2P mode near the tip, with a 2S mode near the pivot, in what is a *2S-2P hybrid mode*, of the kind first observed by Techet *et al.* (1998) for the controlled oscillations of a tapered cylinder in a free stream. The vorticity measurements, in figure 12, show this hybrid mode, and it is found that the vortex splitting that must take place, between the cells of 2S and 2P, occurs at a location around 82%–85% from the pivot in this example. The division based on the Williamson–Roshko map of regimes would suggest a cell boundary around 70% along the span, but such cell boundary predictions of what is in reality a three-dimensional vortex dynamics phenomenon is possibly asking too much of the comparisons. Similar predictions compared well with observations in the study by Techet *et al.* (1998), whose tapered cylinder spanned the 2S and 2P regimes in the Williamson & Roshko (1988) map of modes. Unlike the vortex dislocations in the wake of a static cylinder (see Williamson 1996), which occur at a beat frequency between spanwise cells of different frequency, this vortex splitting is locked to the frequency of oscillation of the cylinder. A three-dimensional image of a vorticity surface for the 2S-2P hybrid mode is included later in figure 17.

This section has indicated, even though in an approximate manner, that the Williamson–Roshko map of modes can be used to suggest the modes of vortex wake formation that will occur along the span of a three-dimensional body, namely the pivoted cylinder case studied here. This is consistent with the results of

(*a*) 2P mode near tip

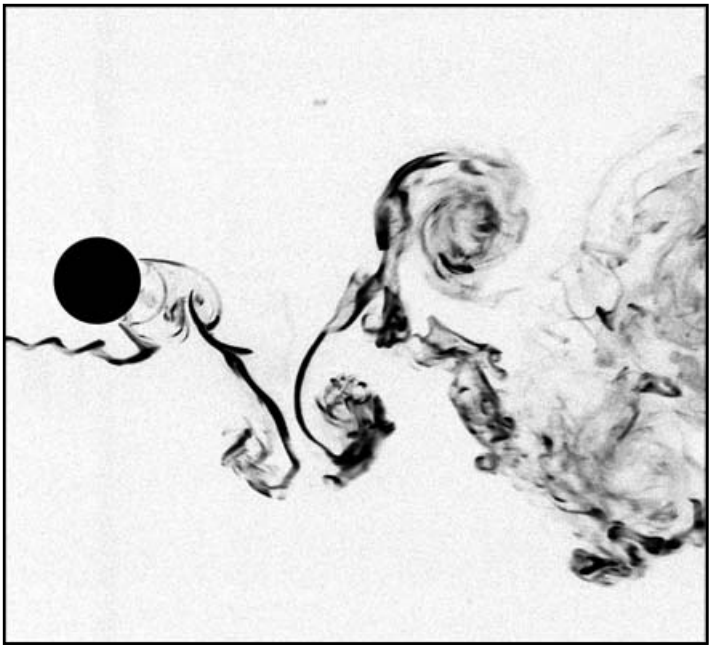

(*b*) 2S mode near pivot

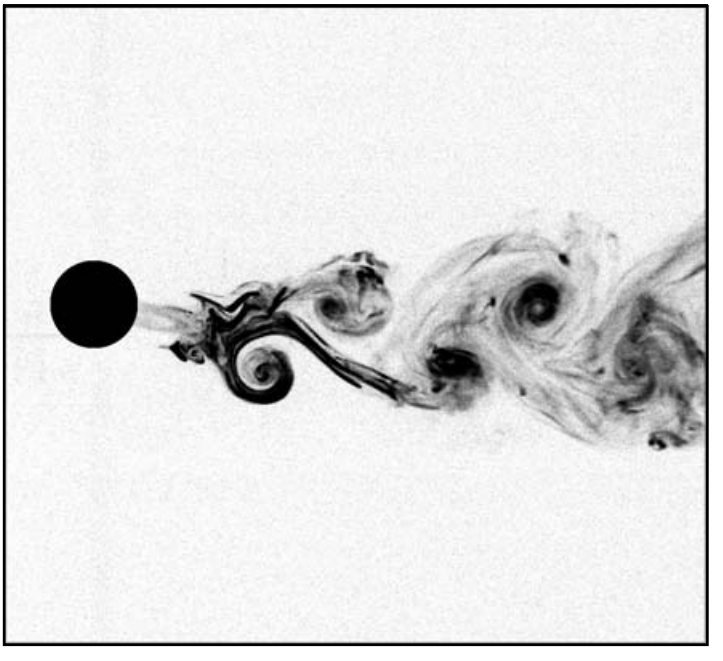

FIGURE 11. Photographs of laser-induced-fluorescence flow visualizations showing the 2P and 2S mode coexisting along the span of the aluminium cylinder ($I^* = 2.68$) at $U^* = 5.67$ and $A_Y^* = 0.91$.

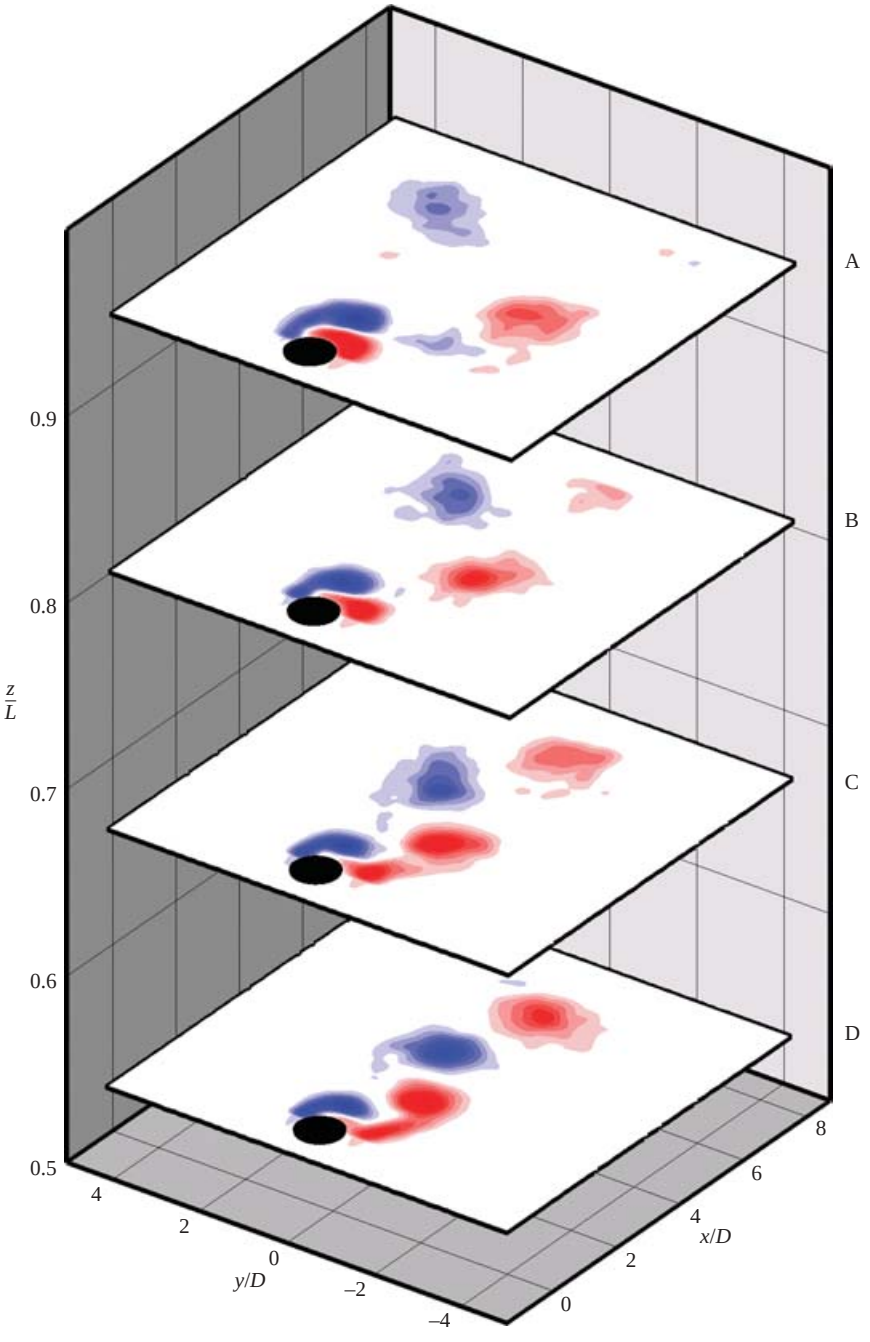

FIGURE 12. An example of the 2S-2P hybrid mode. Contours of vorticity are shown at different z/L-positions of the aluminium cylinder ($I^* = 2.68$) in the initial branch. The cylinder has just passed the point of maximum transverse amplitude in the cycle. Blue represents clockwise vorticity, while red corresponds to counterclockwise vorticity. The contour levels are $\omega D/U = \pm 0.3, \pm 0.6, \pm 1.0, \pm 1.5, \ldots, \pm 5.0$. $U^* = 5.67$, $A_Y^* = 0.91$, DPIV layers A, B, C, D. We should point out that the pivot is below the bottom of the diagram, at $z/L = 0$.

Techet *et al.* (1998) who pioneered the use of this map of modes to predict wake patterns for three-dimensional configurations. It is possible that the map could be used in other configurations such as vibrating cables and cantilevers. However, the validation of the 'quasi-uniform' amplitude assumption appears to be confined to cases where the dynamics do not involve significant streamwise motion. One might expect a departure from such predictions in the case where there is significant streamwise motion, as we find in the upper branch (see figure 9), and presented in the next sub-section.

4.2. *Vortex dynamics with large streamwise oscillations*

With streamwise vibration amplitudes of the order of 35% of the transverse amplitude, one might suspect vortex wake modes to be different to those found for strictly transverse vibrations, for example those patterns found for the uniform-amplitude configuration. If we look now at figure 13, we see immediately a markedly different vortex wake mode comprising pairs of like-signed vortices forming in each half-cycle of cylinder motion. Two co-rotating vortex pairs are formed per cycle, in what may be called a *2C-mode*, consistent with the terminology introduced in Williamson & Roshko (1988). While the two vortices at the tip of the cylinder merge quickly in the near-wake region, such vortices, further along the span towards the pivot, rotate around each other and one expects them to merge further downstream. (The expectation of merging further downstream is based on many vortex interaction studies. References to this phenomenon, and an explanation of the physical mechanism for merging can be found in Cerretelli & Williamson 2003).

A time sequence showing the vortex dynamics during a cycle of body motion is shown in figure 14, corresponding to layer D in the previous figure. The phase-averaged DPIV images are separated by a quarter-period of the oscillation cycle. The maximum transverse amplitude is indicated by a dashed line, while the amount of streamwise motion is noticeable from the x-deviation of the cylinder centre from this line. There are clearly two pairs of co-rotating vortices of roughly equal strength shed per cycle. The vortices comprising each pair start to rotate around each other while they travel downstream. A vortex split along the span occurs again in this mode, as for the 2S-2P hybrid mode. However, in this case the vortex dislocation leads to co-rotating pairs of vortices, rather than to counter-rotating vortex pairs.

Observing the vortex dynamics in figure 13, one might assume that we do not have a 2C mode, but more like a 2S-2C hybrid mode, i.e. a single vortex nearer the tip in each half-cycle, transforming into a co-rotating pair as we approach the pivot. However, this is not the case, as a close-up study of the vortex formation in figure 15 reveals. (In this plot, time increases down the page.) For layer B, nearer the tip, two vortices (1 and 2) are indeed formed in the near wake, but it happens that they merge rapidly in the near wake, whereas further along the span, in layer D, the vortices marked 1 and 2 remain as distinct entities (a co-rotating pair), as they travel downstream in this figure. Therefore the designation of a 2C mode reflects the existence, near the body, of two pairs of co-rotating vortex pairs all along the span, per cycle of oscillation.

The distribution of the normalized circulation $\Gamma^* = \Gamma/UD$ along the span of the cylinder is computed for the 2C mode. For this purpose, the vorticity (for a particular time which corresponds to the fourth frame in figure 15) is evaluated along the complete span. At this time during a cycle, the cylinder has just passed the maximum displacement, leaving vortex 1 and vortex 2 completely shed from the cylinder. The value of circulation is presented in table 2, as a function of z/L. The total circulation

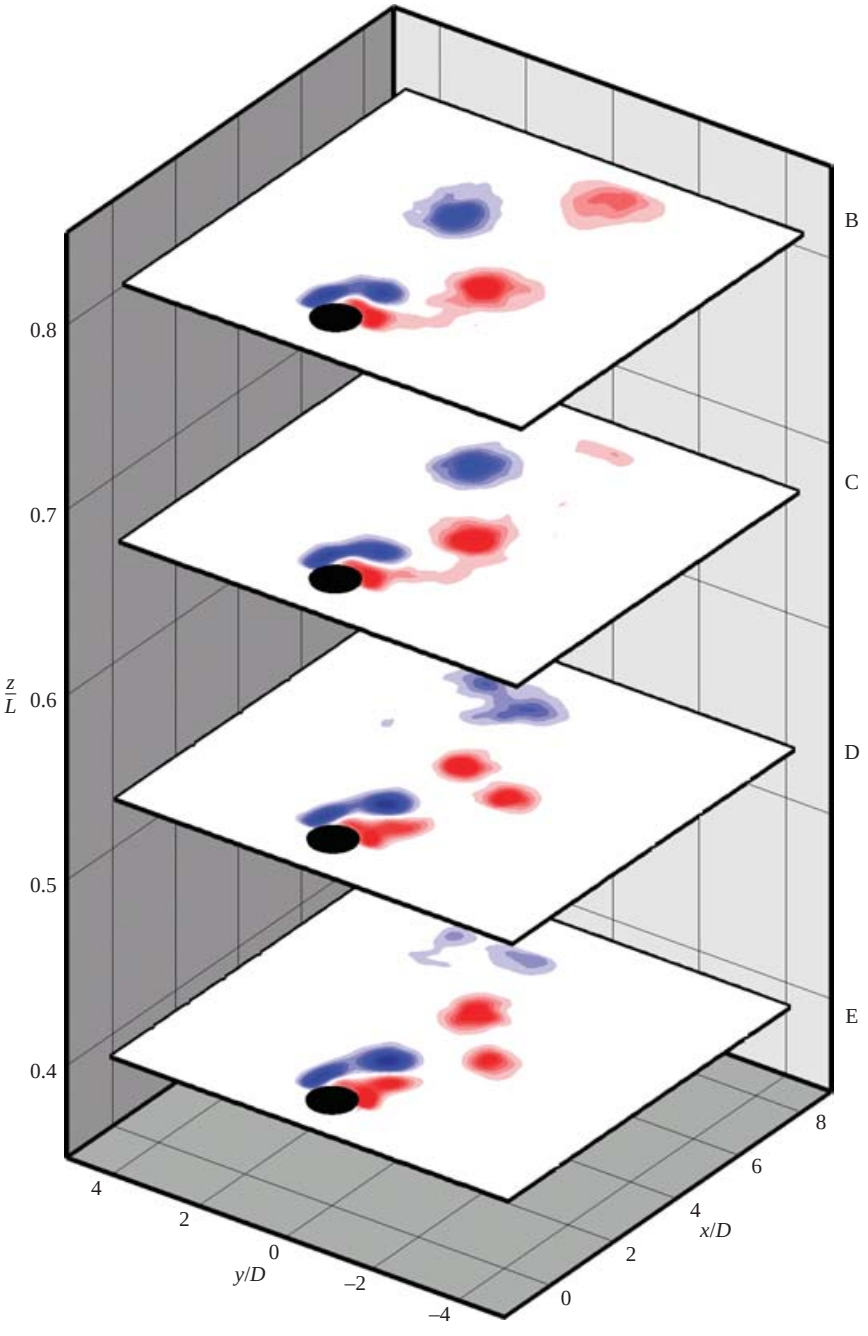

FIGURE 13. An example of the 2C mode. Contours of vorticity are shown at different z/L-positions of the plastic cylinder ($I^* = 1.03$) in the upper branch. The cylinder is moving towards the zero crossing in the cycle. The contour levels shown are $\omega D/U = \pm 0.5, \pm 1.0, \pm 1.5, \ldots, \pm 5.0$. $U^* = 6.15$, $A_Y^* = 1.12$, DPIV layers B, C, D, E. We should point out that the pivot is below the bottom of the diagram, at $z/L = 0$.

per half-cycle (combining vortices $1 + 2$) slightly increases, as one travels from the pivot to the tip. This is expected, since the amplitudes of oscillation get larger, and the rate of circulation production is roughly proportional to the instantaneous square

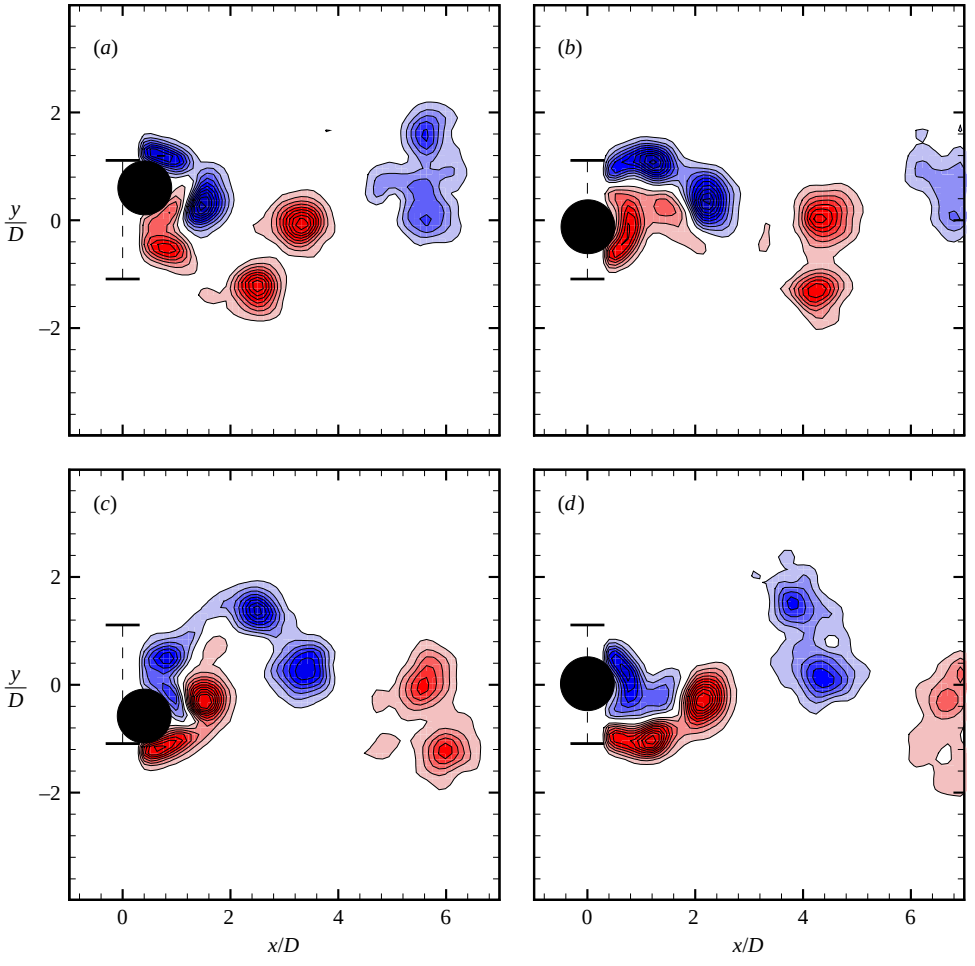

FIGURE 14. Evolution of the 2C mode in time during one oscillation cycle of the plastic cylinder. The dashed lines indicate the extent of the transverse amplitudes. (DPIV layer D, $\Delta t/T = 1/4$, parameters same as in figure 13).

of the relative velocity of the body through the fluid. The circulation strength Γ^* of the two co-rotating vortices $(1+2)$ agrees well with the total circulation of the strong and weak vortex in the case of uniform amplitude as studied by Govardhan & Williamson (2000). Their value for the upper branch is $\Gamma^* \approx 2.85 + 0.60 = 3.45$ and for the lower branch $\Gamma^* \approx 2.85 + 1.7 = 4.55$.

5. Equations of motion and the existence of a critical inertia

In this section, in analogy with a parallel study for an XY motion cylinder (uniform amplitude), we will make use of a pair of simple equations of motion to describe the dynamics of the pivoted body in both the X-direction and Y-direction. (The presentation and solutions for these equations are contained in Appendix B, rather than in the main body of the text, to streamline the presentation in this section.) By using these equations, certain relationships between the X and Y motions will be deduced, and one of the key ingredients leading to these relationships is the fact that,

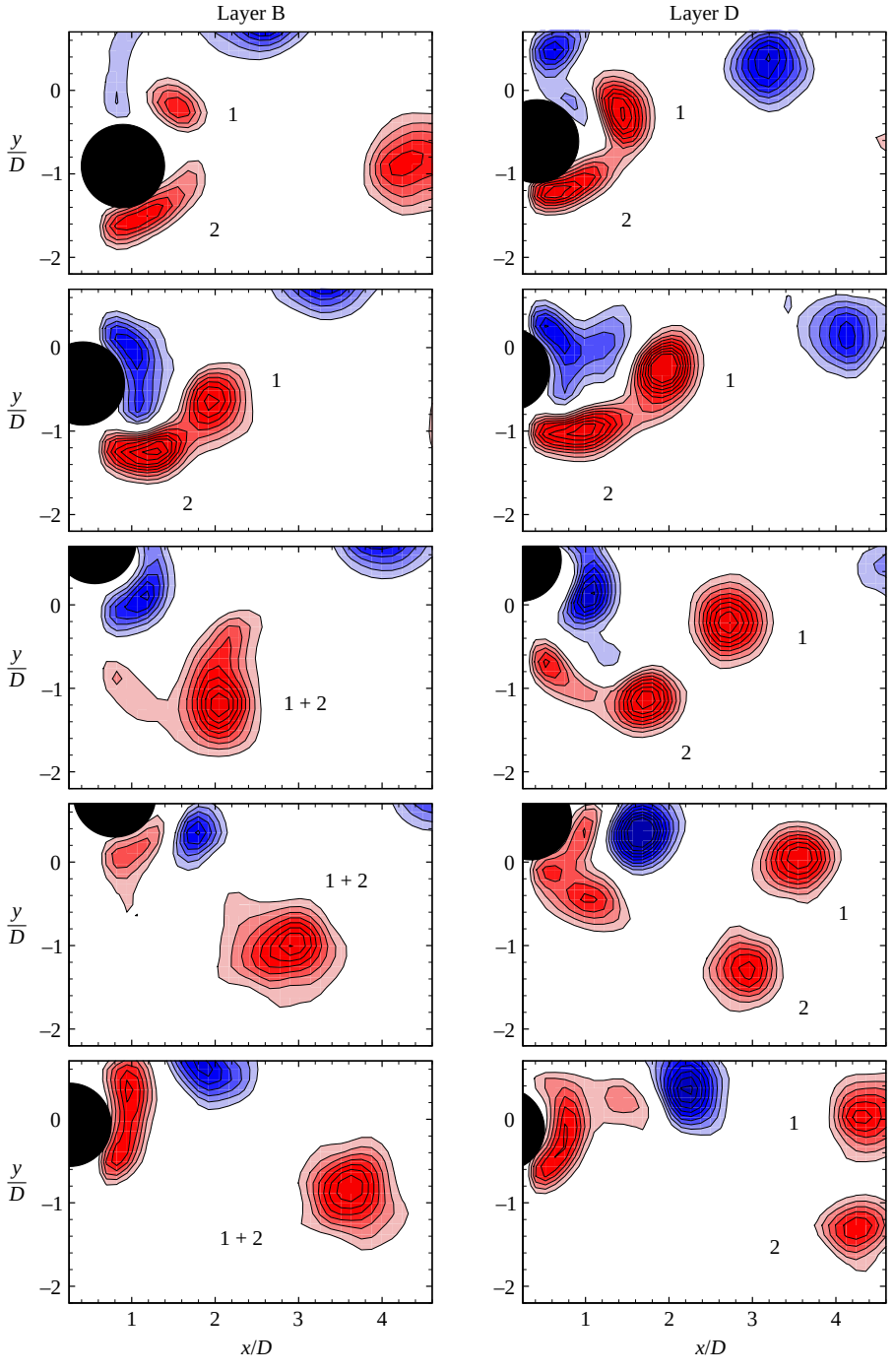

FIGURE 15. Comparison of the vortex shedding process of the 2C mode in the DPIV layers B and D, showing the vortex merging of the two co-rotating vortices in layer B early in the cycle. Time increases down the page. (Contour levels $\omega D/U = \pm 1.0, \pm 1.5, \ldots, \pm 5.0$; $\Delta t/T = 1/5$, other parameters same as in figure 13).

Layer	z/L	1	2	$(1+2)$
A	0.95	–	–	4.26
B	0.81	–	–	4.08
C	0.68	–	–	3.85
D	0.54	1.94	1.77	3.71
E	0.40	2.47	1.50	3.97
F	0.26	2.60	1.15	3.75

TABLE 2. Circulation (Γ^*) of the anticlockwise vortices shed by the 2C mode in one half-cycle of the cylinder motion. The column $(1+2)$ indicates the sum of the two single vortices in columns 1 and 2. The absence of values given for vortex 1 and 2 indicates that they have merged. The values have an error estimated to be $\Delta\Gamma^* = \pm 0.20$.

for periodic vibrations, the streamwise oscillation frequency (f_X) is twice that for the transverse direction (f_Y): $f_X = 2f_Y$. We shall find that there exists a critical inertia (I^*_{crit}), below which the large-amplitude vibrations will persist, up to infinitely high normalized velocities, U^* (in theory). We evaluate the critical inertia for the present pivoted body dynamics.

Similar equations to those found in Appendix B have been discussed extensively for Y-only motion in Govardhan & Williamson (2000); in particular the equation for the frequency of the system formed the basis of much discussion. It was found, for an extensive set of experiments, that an excellent functional relationship between the frequency of the lower response branch $f^*_{Y\,lower}$ and m^* could be deduced. The relationship was found to be accurately represented by the equation

$$f^*_{Y\,lower} = \sqrt{\frac{m^*+1}{m^*-0.54}}. \tag{5.1}$$

This equation led to the discovery of a critical mass, $m^*_{crit} = 0.54$, below which the lower branch ceases to exist. What happens is that the response amplitude of the upper branch persists to infinite normalized flow velocities, if $m^* < m^*_{crit}$ (as proven later in independent experiments by Govardhan & Williamson 2002). One of the questions we have here for the pivoted body is: does a critical inertia exist also for this type of system?

Essentially, one finds here in a manner like the uniform-amplitude cylinder, that the value of the effective added inertia coefficient C_{EAy} diminishes till it reaches a certain minimum and negative value at the end of the synchronization regime, which we shall define as $(C_{EAy})_{crit}$. The variation of C_{EAy} as a function of $(U^*/f^*)S$, through the synchronization regime, is shown in figure 16. The system cannot operate at a value of $(-C_{EAy})$ that is greater than the inertia ratio I^*, otherwise the denominator inside the square-root equation (B 15) for the frequency f^*_Y becomes negative. In essence, if $I^* < (C_{EAy})_{crit}$, and one increases U^* to large values, one tends towards an 'operating point' such that the value of the effective added mass matches the given inertia ratio I^*:

$$C_{EAy} = -I^*. \tag{5.2}$$

As normalized velocity U^* becomes large, so the frequency (f^*) also becomes large (from equation (B 15), where the denominator becomes small), and one approaches the point where equation (5.2) holds, in the plot of figure 16. This would fix the value of $(U^*/f^*)S$, and therefore, from the response amplitude plot for the particular system, for example figure 8, one would fix the vibration amplitude that would persist

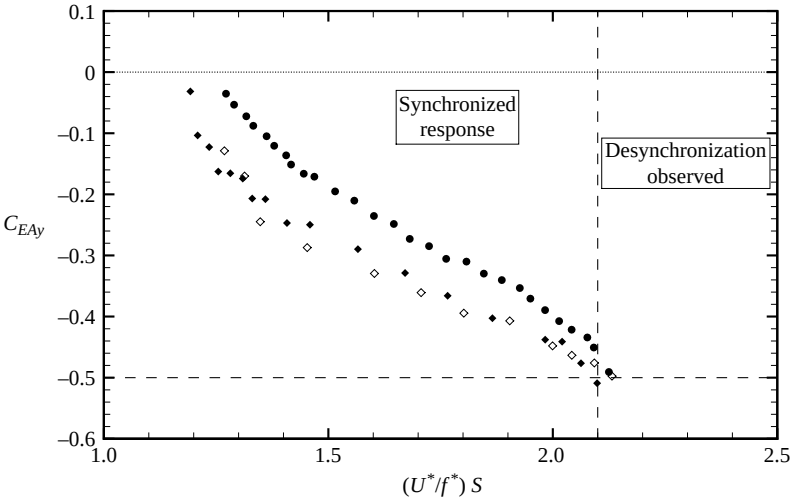

FIGURE 16. Negative effective added inertia coefficient C_{EAy} of the plastic and the aluminium cylinder as a function of the 'true' reduced velocity $(U^*/f^*)S$ up to the point of desynchronization, suggesting the existence of a critical value, given approximately by $(C_{EAy})_{crit} \approx -0.5$. (●, diameter 9.6 mm) plastic $I^* = 1.03$, (◆, 12.8 mm; ◇, 25.4 mm) aluminium $I^* = 2.68$.

for large U^*. For a more comprehensive description of such a phenomenon, the reader is referred to Govardhan & Williamson (2000, 2002). In the present case, the critical inertia ratio (or the maximum value of the inertia ratio where this phenomenon would occur) is given by the minimum value of C_{EAy} within the synchronization regime in figure 16, so that rather approximately

$$I^*_{crit} \approx 0.5. \tag{5.3}$$

Any value of the inertia that is reduced to below the magnitude of this I^*_{crit} would exhibit an infinitely wide regime of synchronized vibrations. The equations in the Appendix (B 15–B 17) also show that, for any positive $I^* < I^*_{crit}$, $C_{EAx} = C_{EAy}$, and therefore that synchronized streamwise motions also will persist to infinite velocity U^*.

Although this phenomenon of an infinite regime of resonance is similar to what was deduced for the uniform-amplitude case, in practice the pivoted cylinder case is more complex than predicted from the equations described above. Obviously, if one approaches large U^* solely by increasing dimensional velocity U, then the mean drag will push the tip over to large angles, and make the required analysis more complex. However, it is theoretically possible to approach large U^* by diminishing the spring stiffness, and thus diminish frequency f_N, to achieve large U^*.

Finally, it would be useful to evaluate the non-dimensional moment $\mathscr{M}^*_i$ and so to predict body motions, by determining the fluid forces on a quasi-uniform basis, using a uniform-amplitude cylinder database. One should note that this is a feedback system requiring the matching of forces and corresponding motions, which are functions of each other, to converge to one or more solutions. However, the database would be prohibitively large, since one would need to fill a volume, like that represented by the three–dimensional response plot in figure 9, with measurements of force and phase. One could, however, reasonably predict pivoted body motions if the streamwise motion is negligible, based on data sets in the plane of A^*_Y and $(U^*/f^*)S$. At the same

time, one would interrogate the 'quasi-uniform' amplitude assumption. This could be extended to other flexible bodies such as cantilevers or cables. Perhaps one reasonable approach to some of these problems is to simulate computationally this flow, either at low Re using DNS, or at higher Re, using large-eddy simulation. Much ongoing work is being done by the group of George Karniadakis at Brown University (see for example: Lucor *et al.* 2001), and by Mike Graham at Imperial College (see for example: Willden & Graham 2001) to simulate such complex flows.

6. Conclusions

Most of the studies into vortex-induced vibrations have been associated with cylinders oscillating transverse to a fluid flow (Y-motion). There are very few papers studying the more practical case of vibration in two degrees of freedom (XY-motion), where the mass and natural frequencies are precisely the same in both X- and Y-directions, or the case where there is variation of amplitude along the span of a body. We have designed the present pivoted cylinder apparatus to investigate both of these effects, as a fundamental problem which represents the simplest configuration having a spanwise variation of amplitude. One central question concerns how well the results from Y-motion studies carry over to the case of a body in two degrees of freedom, where there is spanwise amplitude variation, i.e. how good is the quasi-uniform assumption?

For moderate values of the product: inertia–damping (or $I^*\zeta$), the system exhibits two amplitude response branches, and for sufficiently low ($I^*\zeta$), three response branches appear, in strong analogy with previous results for Y-motion bodies. In the case of moderate $I^* \sim 10$, the pivoted cylinder response to vortex-induced forces is principally transverse to the flow. When plotted in the Williamson & Roshko (1988) map of modes (valid for strictly transverse motion), one expects reasonable prediction of the spanwise vortex wake modes based on this map. The same is true of a light body, regarding the initial and lower response branches. In these cases above, the 'quasi-uniform' assumption, employing transverse-only data, would appear reasonable. However, if the body is sufficiently light to allow the upper branch to appear, then we find this branch is associated with significant streamwise motion just as one finds for uniform-amplitude XY-motion cylinders (Jauvtis & Williamson 2004*a*, *b*). In this case, a marked departure in the mode of vibration and vortex wake mode is found, compared with predictions based on the Williamson–Roshko map of modes. The assumption that one could employ Y-only force date would thus not hold well.

The conditions where such an assumption holds in this pivoted cylinder flow as well as in flows around flexible bodies, such as cantilevers and cables, is important. Employment of force coefficients from uniform-cylinder data is part of several commercial programs which predict riser tube dynamics in the ocean, usually utilizing Y-only force data. In the presence of significant streamwise motion, the quasi-uniform approach requires a force-coefficient data set from controlled XY-motions which would be prohibitively large, as it would depend on several different parameters (A_X^*, A_Y^*, θ, f^*, for example). In that case, the approach of employing scaled experiments and numerical simulations would be a useful guide.

The response branches for the bodies with low ($I^*\zeta$) correspond with both of the well-known vortex wake modes; namely the 2S mode (two single vortices per cycle) and 2P mode (two vortex pairs per cycle) along the span. We also observe a clear 2S-2P hybrid mode, similar to that found for vibrating tapered cylinders by Techet *et al.* (1998). These different modes correspond well with the Williamson & Roshko

(1988) map of modes in the plane of normalized amplitude and velocity, so long as the streamwise vibration is small. However, when the inertia of the body is sufficiently small, the correspondence with the map of modes is not close. The response branches cross over each other in this map, and one has to introduce a third dimension to represent streamwise amplitude. This three–dimensional plot shows that the two response branches exist in quite different parameter spaces.

In the case of the lightest bodies, we find much larger transverse amplitude, as well as significant streamwise vibrations, corresponding to a new vortex formation mode, which comprises two co-rotating vortices each half-cycle, defined as a '2C' mode. The principal three-dimensional vorticity structures corresponding to each vortex wake mode have been constructed, based on measurements of vorticity at several cross-sections along the span, and are shown, with the complex 2S-2P hybrid mode in figure 17. Vortex dislocations (or vortex splitting) are associated with the 2C mode, as well as the 2S-2P hybrid mode; in one case leading to co-rotating vortex pairs, and in the other case to counter-rotating vortex pairs. In the case of the 2C mode, we also observe vortex merging in the near wake.

It appears that the 2C mode is the fourth vortex wake mode which contributes to vortex-induced vibration of such cylindrical structures. We summarise, in figure 18, the set of four vortex wake modes:

$$\{2S, 2P, 2C, 2T\}$$

all of which have an antisymmetric symmetry. The 2T mode comprises the formation of two triplets of vortices in each half-cycle, and is found in the XY-motion of uniform-amplitude cylinders in Jauvtis & Williamson (2004*a*, *b*). The 2C mode is found in the present pivoted body experiments. The 2S and 2P modes are found in all cases including the transverse-only cylinder vibration. All of these vortex wake modes are generated by the body motion, while the vortices in turn provide positive energy transfer to continuously support the body motion.

We introduce equations of motion for the case of the pivoted cylinder with two degrees of freedom, and thereby deduce that a critical inertia, I_{crit} exists (analogous to the 'critical mass' of Govardhan & Williamson 2000, 2002), below which the pivoted body is predicted to have an infinitely wide regime of flow velocities where resonant oscillations will occur.

The present results and phenomena are expected to represent some of the fundamental features associated with more complex flows such as the vortex-induced vibrations of cables. In an approximate manner, one might expect the vortex-induced vibrations of the pivoted cylinder to be similar to the body motions and wake dynamics between a node and antinode of a standing wave pattern for a cable, for example. The present results then suggest conditions under which the 2S and 2P, and hybrid modes occur along the span, with their corresponding induced forces and energy transfer to body motion. In the context of cable vortex-induced vibrations, interesting results concerning the existence of vortex dislocations (which would occur for a hybrid 2S-2P mode) have been uncovered from numerical simulations by Lucor *et al.* (2001). Higher-amplitude vibrations, and the possible existence of a 2C mode with significant streamwise motions, have not yet been observed in contexts such as the vibrating cable or cantilever.

Finally, it remains an open question as to how well such laboratory-scale experiments, as presented here for example, carry across to much higher Re, and indeed to full-scale structures. This question has recently been discussed in the review paper by Williamson & Govardhan (2005), where further references may be found on

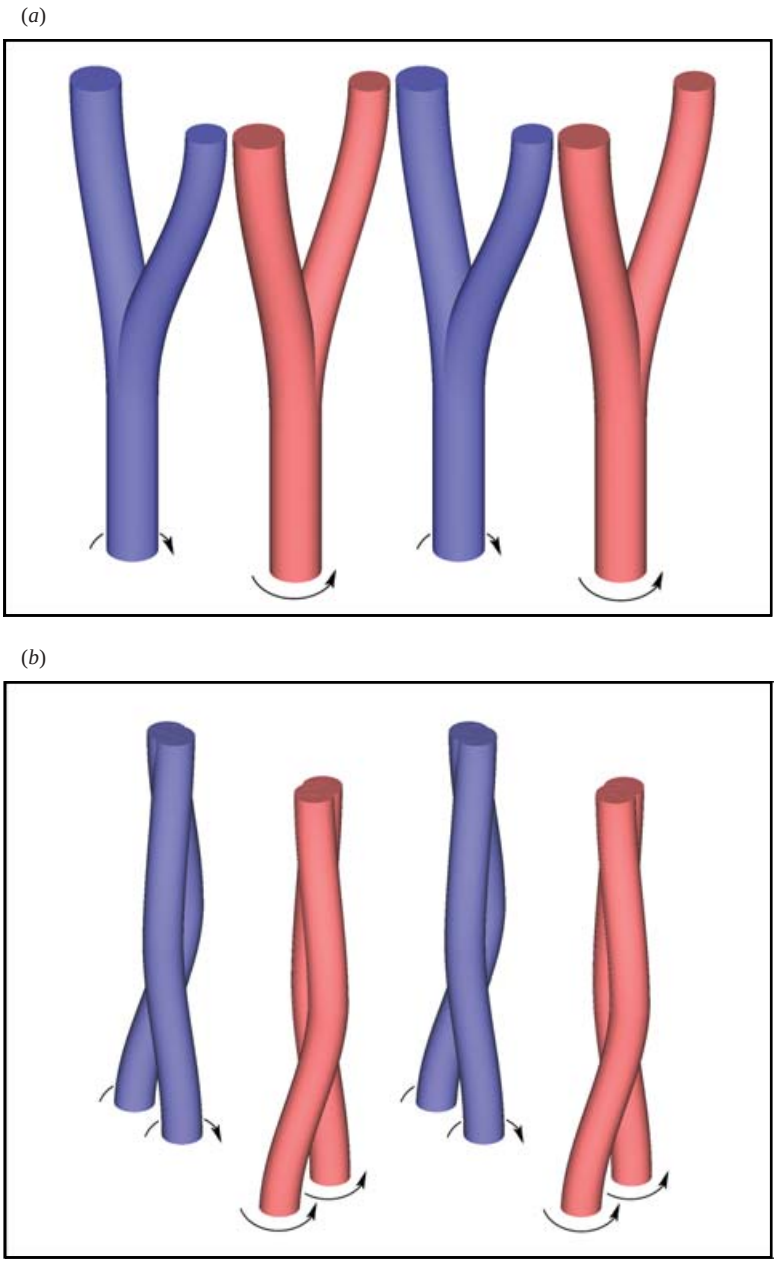

FIGURE 17. Three-dimensional models of the two new modes of vortex formation, constructed on the basis of the DPIV vorticity layers. The pivot point of the cylinder is towards the bottom of the diagrams and the fluid is moving from the left to the right. (*a*) 2S-2P hybrid mode, (*b*) 2C mode.

this point. Exciting evidence to date has been presented by Triantafyllou, Hover & Techet (2004), where the accumulated high- Re results suggest that low- Re phenomena (such as the response amplitude levels, vortex formation modes, etc.) do indeed carry across to high Re, even up to postcritical $Re \sim 10^6$, although some of the results need further confirmation, and publication in the open literature.

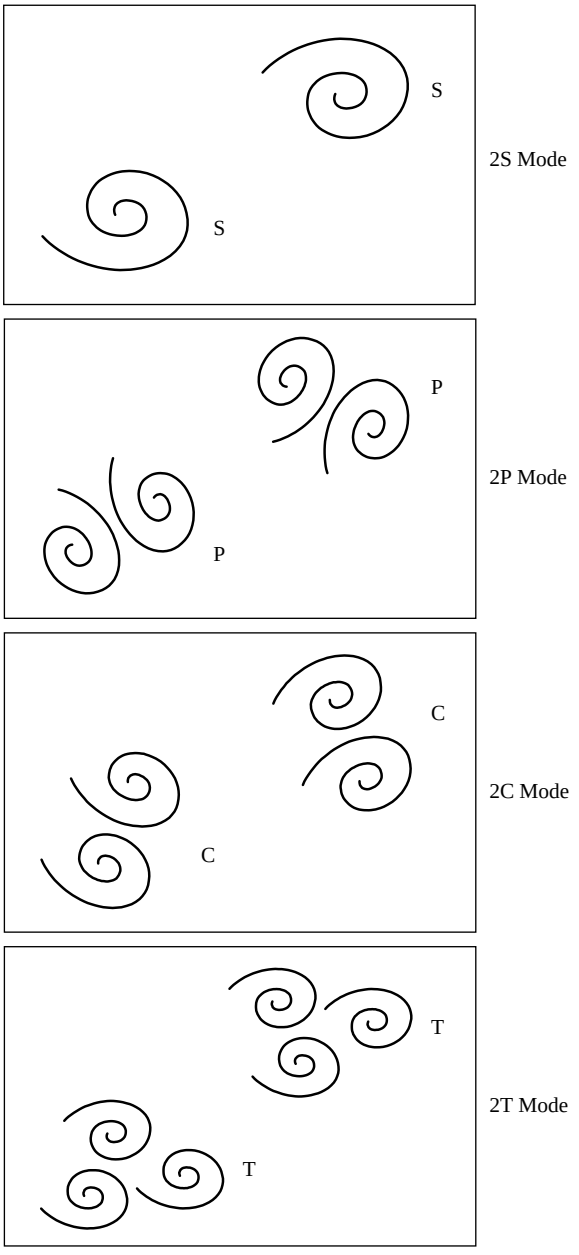

FIGURE 18. Diagram of vortex patterns found in free vortex-induced vibrations of cylindrical structures with one and two degrees of freedom.

The support from the Ocean Engineering Division of ONR, monitored by Dr Tom Swean, is gratefully acknowledged (ONR. Contract Number N00014-95-1-0332). The work of Felix Flemming was also supported by the German Academic Exchange Service (DAAD), 2000. We have benefited greatly from many discussions with Dr Raghuraman Govardhan, Dr Nathan Jauvtis, Dr Chantal Champagne, and Evi Zeitlmayr. The principal components of this study were completed during the visit to Cornell University of Felix Flemming during the academic year 1999–2000, and

involved further visits in Summer 2001 and 2002 to complete the PIV and other aspects. The support by Professor Dr.-Ing. Johannes Janicka at the Institute for Energy and Powerplant Technology, Darmstadt University of Technology is also gratefully acknowledged.

Appendix A. The 2S and 2P modes for the pivoted cylinder

In this Appendix we present the evidence for the existence of the 2S and 2P modes along the span of the pivoted cylinder, under particular conditions. These are placed as an Appendix, since they are well-known to occur in the uniform-amplitude case, and we wish to streamline the presentation of the new modes in the main text of the paper. In figure 19, an example of the 2S mode is given, while figure 20 provides a view of the 2P mode along the span. These examples of such modes come from both the plastic cylinder and the aluminium cylinder. Finally figure 21 compares the two modes from the present pivoted body case to the uniform-amplitude modes from other studies, exhibiting a marked agreement.

Appendix B. The equations of motions

We present here two equations of motion for the pivoted cylinder with two degrees of freedom. These equations of motion are defined in terms of an angular deflection α, since the cylinder is moving as a pendulum, and they are obtained by balancing the moments with respect to the pivot point. Due to the small deflections ($\alpha \ll 1$) of the cylinder, and its length being much bigger than the diameter $L \gg D$, the equations can be linearized, and then written as follows:

$$I\,\ddot{\alpha}_i(t) + c\,\dot{\alpha}_i(t) + k\,\alpha_i(t) = M_i(t). \tag{B 1}$$

Here the subscript i stands for the X- or the Y-direction. The representative model, on which these equations are based, is presented in figure 22(a). The cylinder mount via the small steel spring pin is treated as a pivot point with an axisymmetric torsion spring of stiffness k_{pin} and a structural damping c. Around this point the cylinder is free to oscillate like a pendulum in any direction perpendicular to its axis. The deflection from the z-direction (aligned with the gravity vector $\boldsymbol{g}$) is described as a function of time by the angle $\alpha_i(t)$. The cylinder has density ρ_c and therefore mass $m = \pi\rho_c D^2 L/4$, that is uniformly distributed along the span. This leads to a moment of inertia I about the pivot point, which is independent of the oscillation direction, and is given by

$$I = \frac{m}{12}\left(\frac{3}{4}D^2 + 4L^2\right) \xrightarrow{L \gg D} I \approx \frac{m}{3}L^2. \tag{B 2}$$

The stiffness k in equation (B 1) is a combination of the structural spring stiffness k_{pin} and the restoring moment due to the weight $\boldsymbol{G}$ and the buoyancy $\boldsymbol{B}$ acting on the cylinder. This restoring moment is proportional to cylinder deflection (if linearized), and is included in total stiffness k as follows (noting m_d is the displaced fluid mass):

$$k = k_{pin} + (m - m_d)g\,\frac{L}{2}. \tag{B 3}$$

It now remains to consider the forcing moment $M_i(t)$ on the right-hand side of the equation. This is interpreted as the integral of the fluid forces per unit

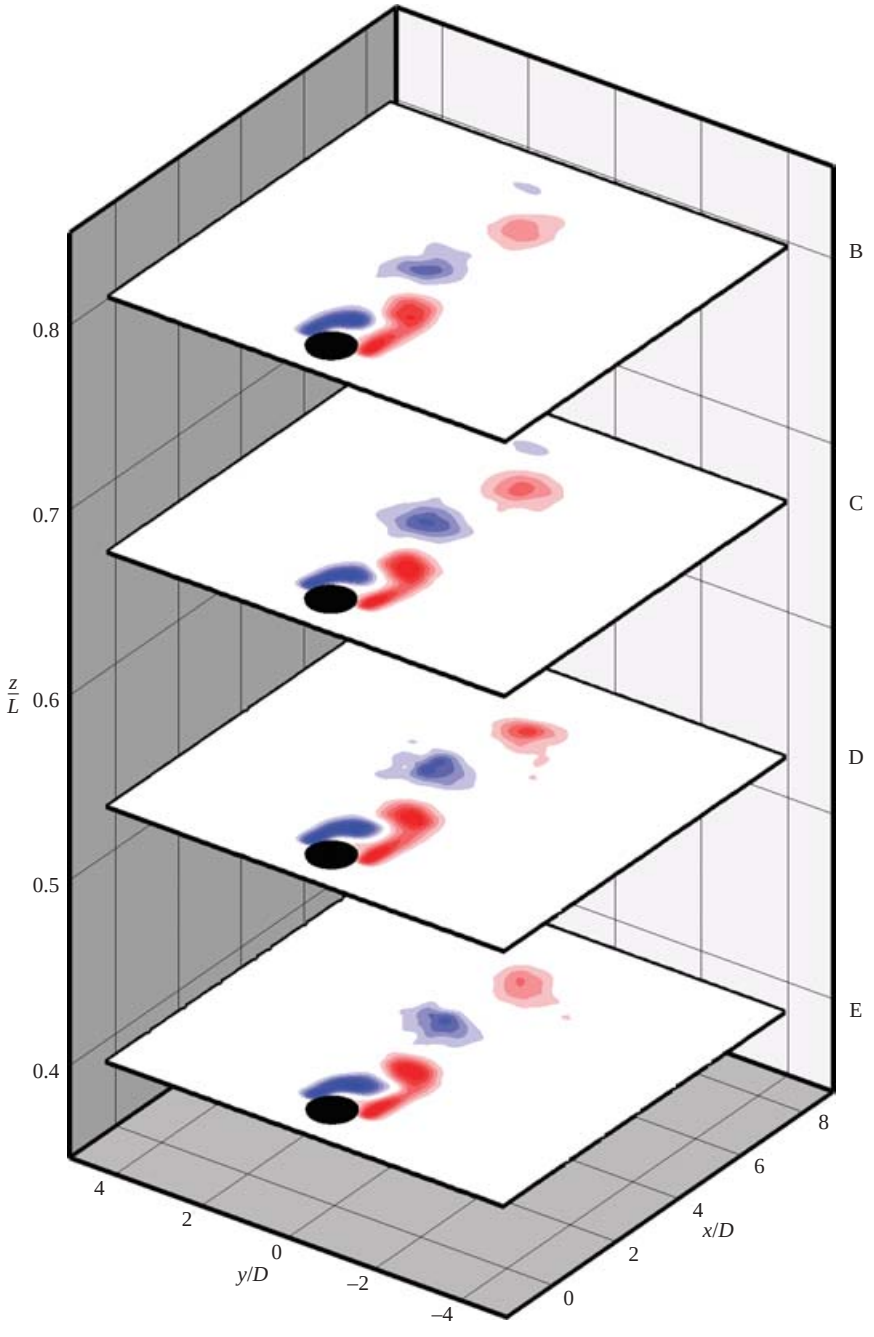

FIGURE 19. An example of the 2S mode all along the span of the pivoted cylinder. Contours of vorticity are shown at different z/L-positions of the plastic cylinder ($I^* = 1.03$) in the initial branch. The cylinder has just passed the point of maximum transverse amplitude in the cycle. The contour levels shown are $\omega D/U = \pm 0.5, \pm 1.0, \pm 1.5, \ldots, \pm 5.0$. $U^* = 3.99$, $A_Y^* = 0.28$, DPIV layers B, C, D, E. We should point out that the pivot is below the bottom of the diagram, at $z/L = 0$.

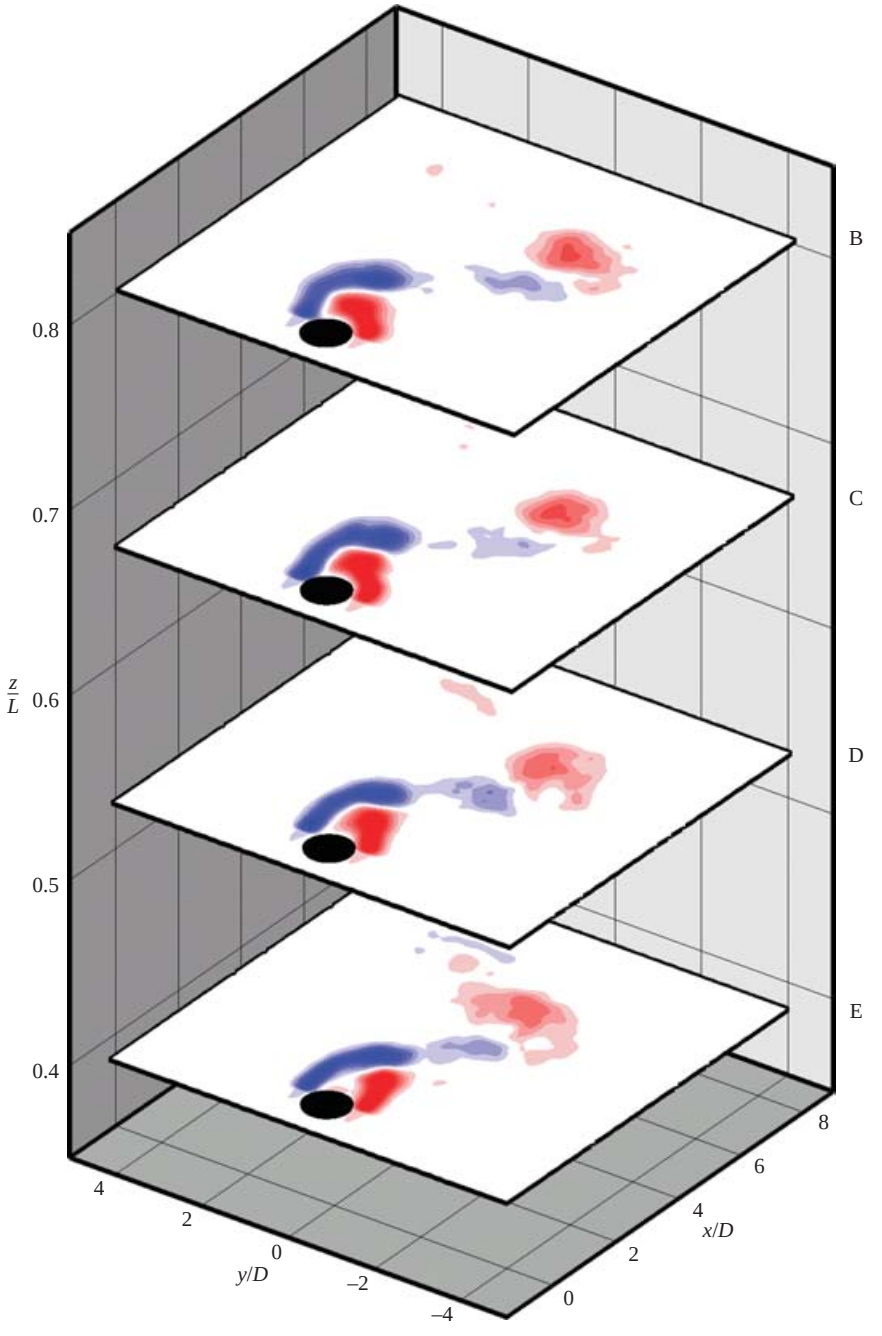

FIGURE 20. An example of the 2P mode all along the span of the pivoted cylinder. Contours of vorticity are shown at different z/L-positions of the aluminium cylinder ($I^* = 2.68$) in the lower branch. The cylinder is moving towards the zero crossing in the cycle. The contour levels are $\omega D/U = \pm 0.3, \pm 0.6, \pm 1.0, \pm 1.5, \ldots, \pm 5.0$, $U^* = 8.30$. $U^*/f^* = 1.35$, $A_Y^* = 0.94$, DPIV layers B, C, D, E. We should point out that the pivot is below the bottom of the diagram, at $z/L = 0$.

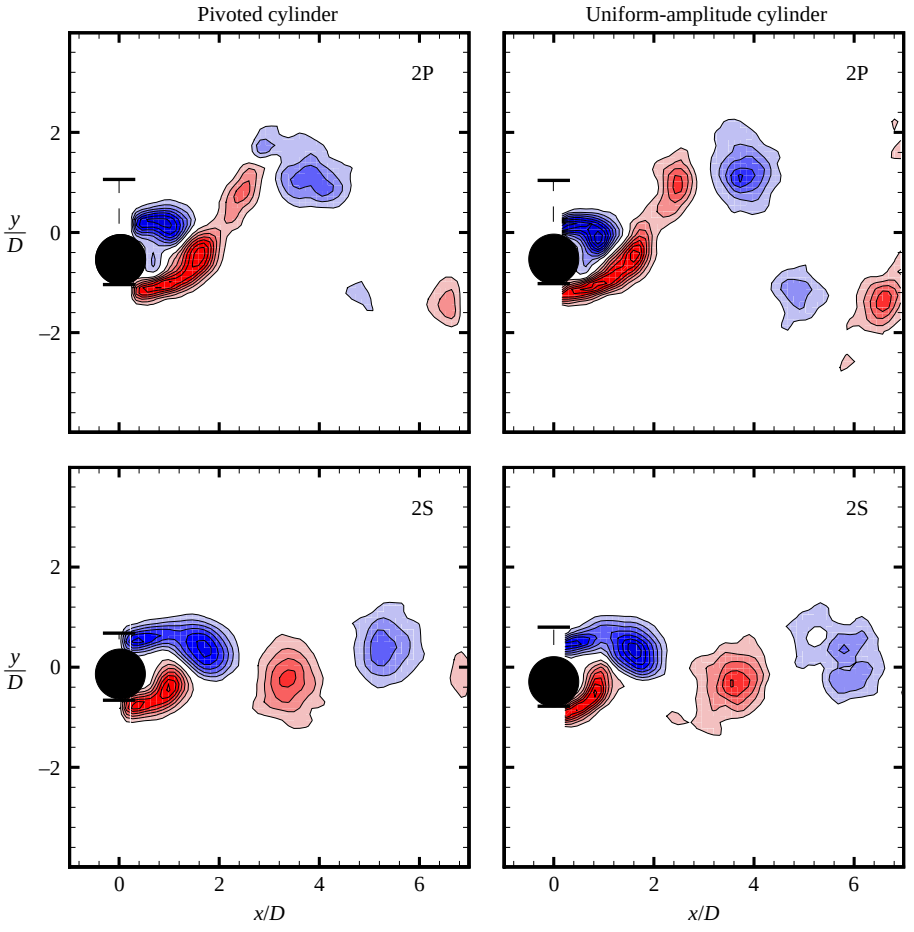

FIGURE 21. Comparison of the 2P and 2S mode of the pivoted cylinder (as in figures 19 and 20) with the elastically mounted rigid cylinder case, presented by Govardhan & Williamson (2000) (2P mode: $U^* = 6.40$, $A_Y^* = 0.60$; 2S mode: $U^* = 5.18$, $A_Y^* = 0.33$). The contour levels are $\omega D/U = \pm 0.5, \pm 1.0, \pm 1.5, \ldots, \pm 5.0$.

length $f_i(z,t)$, multiplied by the lever arm z, over the immersed span of the cylinder:

$$M_i(t) = \int_0^L f_i(z,t)\, z \, \mathrm{d}z. \tag{B 4}$$

We assume that the fluid force $f_i(z,t)$, and the moment $M_i(t)$, are represented well by the following sinusoidal functions, where the amplitudes of these expressions are dependent on spanwise location (z):

$$f_i(z,t) \approx f_{o,i}(z)\, \sin(\omega_i t + \phi_i), \tag{B 5}$$

$$M_i(t) = M_{o,i}\, \sin(\omega_i t + \phi_i) \qquad \text{with} \qquad M_{o,i} \equiv \int_0^L f_{o,i}(z)\, z \, \mathrm{d}z. \tag{B 6}$$

The amplitude of the fluid force per unit length $f_{o,i}(z)$ can be given as:

$$f_{o,i}(z) \equiv \tfrac{1}{2}\, \rho U^2 D C_i(z). \tag{B 7}$$

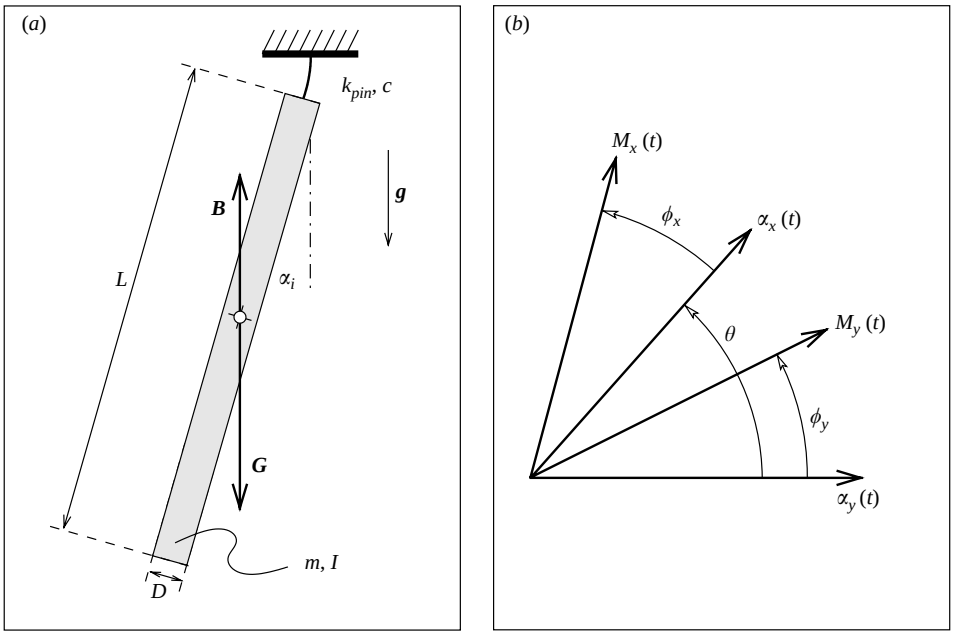

FIGURE 22. (*a*) Definitions of the quantities and (*b*) the phases (in between the positions and forcing) that are used in the presented equations of motion for the pivoted cylinder.

This can be used to express the amplitude of the forcing moment $M_{o,i}$ in terms of given quantities and a non-dimensional integral ($\mathscr{M}_i^*$) over the force coefficient $C_i(z)$. Using a normalized spanwise distance $z^* = z/L$, we write

$$M_{o,i} = \tfrac{1}{6}\,\rho U^2 L^2 D\,\mathscr{M}_i^* \qquad \text{with} \qquad \mathscr{M}_i^* \equiv 3\int_0^1 C_i(z^*)\,z^*\,\mathrm{d}z^*. \tag{B 8}$$

The quantity $\mathscr{M}_i^*$ can be interpreted as a 'moment coefficient' in the two directions X and Y.

We assume solutions of the following form:

$$\alpha_y(t) = \alpha_{o,y}\,\sin(\omega t), \qquad \alpha_x(t) = \alpha_{o,x}\,\sin(2\omega t + \theta), \tag{B 9}$$

$$M_y(t) = M_{o,y}\,\sin(\omega t + \phi_y), \qquad M_x(t) = M_{o,x}\,\sin(2\omega t + [\phi_x + \theta]). \tag{B 10}$$

The different phases that appear in these equations are defined by the phase plot in figure 22(*b*). The oscillation in the transverse direction $\alpha_y(t)$ is the reference motion. The phase between the x- and the y-motion is labelled θ, while the phases between the forcing moments $M_x(t)$, $M_y(t)$ and the corresponding positions $\alpha_x(t)$, $\alpha_y(t)$ are named ϕ_x and ϕ_y respectively. The damping ratio ζ is defined

$$\zeta \equiv \frac{c}{2\sqrt{k(I + I_A)}} \qquad \text{with} \qquad I_A = C_A\,I_d = C_A\,\frac{m_d}{3}L^2, \tag{B 11}$$

where I_A is the potential added inertia due to the body motion in the fluid, and it is given by the added inertia coefficient (C_A) times the inertia of the displaced fluid I_d.

It can be shown that the coefficient C_A is equal and equivalent to the added mass coefficient for the uniform-amplitude cylinder, taking the value 1.0. We may thus define the inertia ratio $I^* = I/I_d$, which is equivalent to the mass ratio $m^* = m/m_d$

of the uniform-amplitude case. If the mass of the pivoted cylinder is uniformly distributed along the span, it is straightforward to show that $I^* = m^*$.

The natural frequency in water f_N is given by

$$f_N = \frac{\omega_N}{2\pi} = \frac{1}{2\pi}\sqrt{\frac{k}{I + I_A}}. \tag{B 12}$$

The ratio between the actual transverse oscillation frequency (f_Y) of the pivoted cylinder and the natural frequency in water (f_N) is defined as frequency ratio $f_Y^* = f_Y/f_N$. From our earlier discussions, $f_X^* = 2f_Y^*$. As mentioned before, for clarity of presentation below, we use f^* to mean transverse normalized frequency f_Y^*.

Substituting equations (B 2)–(B 12) into the equation of motion (B 1) in the X- as well as the Y-direction, and noting the assumption that $\alpha_i \ll 1$, which yields the result $y \approx \alpha_y L$ and $x \approx \alpha_x L$ at the tip of the cylinder, one finds the normalized tip amplitudes, A_Y^* and A_X^*, as follows:

$$A_Y^* = \alpha_{o,y}\left(\frac{L}{D}\right) = \frac{1}{4\pi^3}\,\frac{\mathscr{M}_y^* \sin\phi_y}{(I^* + C_A)\zeta}\,\left(\frac{U^*}{f^*}\right)^2 f^*, \tag{B 13}$$

$$A_X^* = \alpha_{o,x}\left(\frac{L}{D}\right) = \frac{1}{4\pi^3}\,\frac{\mathscr{M}_x^* \sin\phi_x}{(I^* + C_A)\zeta}\,\left(\frac{U^*}{2f^*}\right)^2 (2f^*). \tag{B 14}$$

The quantity $\mathscr{M}_i^* \sin\phi_i$, that appears in both equations, is the component of the moment (due to the distributed total fluid force) in phase with the velocity of the body, and is analogous to the force component $C_Y \sin\phi$ found for the uniform-amplitude case (see for example, Khalak & Williamson 1999). Expressions for the frequencies f_Y^* and f_X^* are also derived from equations (B 1)–(B 12):

$$f^* = \sqrt{\frac{I^* + C_A}{I^* + C_{EAy}}}, \tag{B 15}$$

$$C_{EAy} = \frac{1}{2\pi^3 A_Y^*}\,\left(\frac{U^*}{f^*}\right)^2 \mathscr{M}_y^* \cos\phi_y, \tag{B 16}$$

$$2f^* = \sqrt{\frac{I^* + C_A}{I^* + C_{EAx}}}, \tag{B 17}$$

$$C_{EAx} = \frac{1}{2\pi^3 A_X^*}\,\left(\frac{U^*}{2f^*}\right)^2 \mathscr{M}_x^* \cos\phi_x. \tag{B 18}$$

The quantities C_{EAy} and C_{EAx} are the effective added inertia coefficients, similar to the effective added mass coefficient for the uniform-amplitude case, and these terms are proportional to the component of the moment (due to distributed forces) in phase with the acceleration.

REFERENCES

Bearman, P. W. 1984 Vortex shedding from oscillating bluff bodies. *Annu. Rev. Fluid Mech.* **16**, 195–222.

Brika, D. & Laneville, A. 1993 Vortex-induced vibrations of a long flexible circular cylinder. *J. Fluid Mech.* **250**, 481–508.

Cerretelli, C. & Williamson, C. H. K. 2003 The physical mechanism for vortex merging. *J. Fluid Mech.* **475**, 41–77.

Eisenlohr, H. & Eckelmann, H. 1989 Vortex splitting and its consequences in the vortex street wake of cylinders at low reynolds number. *Phys. Fluids* A **1**, 189–192.

Evangelinos, C. & Karniadakis, G. E. 1999 Dynamics and flow structures in the turbulent wake of rigid and flexible cylinders subject to vortex-induced vibrations. *J. Fluid Mech.* **400**, 91–124.

Evangelinos, C., Lucor, D. & Karniadakis, G. E. 2000 DNS-derived force distribution on flexible cylinders subjected to vortex-induced vibration. *J. Fluids Struct.* **14**, 429–440.

Feng, C. C. 1968 The measurement of vortex-induced effects in flow past stationary and oscillating circular and D-section cylinders. Master's thesis, University of British Columbia, Vancouver, BC, Canada.

Fujarra, A. L. C., Pesce, C. P., Flemming, F. & Williamson, C. H. K. 2001 Vortex-induced vibration of a flexible cantilever. *J. Fluids Struct.* **15**, 651–658.

Govardhan, R. & Williamson, C. H. K. 2000 Modes of vortex formation and frequency response of a freely vibrating cylinder. *J. Fluid Mech.* **420**, 85–130.

Govardhan, R. & Williamson, C. H. K. 2002 Resonance forever: Existence of a critical mass and an infinite regime of resonance in vortex-induced vibration. *J. Fluid Mech.* **473**, 147–166.

Govardhan, R. & Williamson, C. H. K. 2005 Vortex-induced vibration of an elastically-mounted sphere. To appear in *J. Fluid Mech.*

Griffin, O. M. & Ramberg, S. E. 1976 Vortex shedding from a cylinder vibrating in line with an incident uniform flow. *J. Fluid Mech.* **75**, 257–271.

Griffin, O. M. & Ramberg, S. E. 1982 Some recent studies of vortex shedding with application to marine tubulars and risers. *Trans. ASME: J. Energy Resour. Tech.* **104**, 2–13.

Jauvtis, N. & Williamson, C. H. K. 2003 Vortex-induced vibration of a cylinder with two degrees of freedom. *J. Fluids Struct.* **17**, 1035–1042.

Jauvtis, N. & Williamson, C. H. K. 2004*a* A high-amplitude 2T mode of vortex formation, and the effects of non-harmonic forcing in vortex-induced vibration. *Eur. J. Mech.* B-*Fluids* **23**, 107–114.

Jauvtis, N. & Williamson, C. H. K. 2004*b* The effect of two degrees of freedom on vortex-induced vibration at low mass and damping. *J. Fluid Mech.* **509**, 23–62.

Khalak, A. & Williamson, C. H. K. 1996 Dynamics of a hydroelastic cylinder with very low mass and damping. *J. Fluids Struct.* **10**, 455–472.

Khalak, A. & Williamson, C. H. K. 1997 Fluid forces and dynamics of a hydroelastic structure with very low mass and damping. *J. Fluids Struct.* **11**, 973–982.

Khalak, A. & Williamson, C. H. K. 1999 Motions, forces and mode transitions in vortex-induced vibrations at low mass-damping. *J. Fluids Struct.* **13**, 813–851.

King, R. 1974 Vortex excited structural oscillations of a circular cylinder in steady currents. In *6th Ann. Offshore Technology Conf. Houston, TX, USA*, OTC Paper 1948.

Lucor, D., Imas, L. & Karniadakis, G. E. 2001 Vortex dislocations and force distribution of long flexible cylinders subjected to sheared flows. *J. Fluids Struct.* **15**, 641–650.

Moe, G. & Wu, Z.-J. 1990 The lift force on a cylinder vibrating in a current. *Trans. ASME: J. Offshore Mech. Arctic Engng* **112**, 297–303.

Naudascher, E. 1987 Flow-induced streamwise vibrations of structures. *J. Fluids Struct.* **1**, 265–298.

Newman, D. & Karniadakis, G. E. 1996 Simulations of flow over flexible cable: a comparison of forced and flow-induced vibration. *J. Fluids Struct* **10**, 439–453.

Ongoren, A. & Rockwell, D. 1988 Flow structure from an oscillating cylinder. Part 2. Mode competition in the near wake. *J. Fluid Mech.* **191**, 225–245.

Pesce, C. P. & Fujarra, A. L. C. 2000 Vortex-induced vibrations and jump phenomenon: Experiments with a clamped flexible cylinder in water. *Intl J. Offshore Polar Engng* **10**, 26–33.

Sarpkaya, T. 1979 Vortex-induced oscillations. *Trans. ASME: J. Appl. Mech.* **46**, 241–258.

Sarpkaya, T. 1995 Hydrodynamic damping, flow-induced oscillations, and biharmonic response. *Trans. ASME: J. Offshore Mech. Arctic Engng* **117**, 232–238.

Techet, A. H., Hover, F. S. & Triantafyllou, M. S. 1998 Vortical patterns behind a tapered cylinder oscillating transversly to a uniform flow. *J. Fluid Mech.* **363**, 79–96.

Triantafyllou, M. S., Hover, F. & Techet, A. H. 2004 The effect of Reynolds number on VIV: From subcritical to supercritical flow. In *Proc. 8th Intl Conf. Flow-Induced Vibrations, Paris, France, 6–9 July 2004* (ed. E. de Langre & F. Axisa) Ecole Polytechnique.

Van Voorhees, A. & Wei, T. 2002 Three-dimensionality in the wake of a surface piercing cylinder mounted as an inverted pendulum. In *Proc. BBVIV-3 Bluff Body Wakes and Vortex-Induced Vibrations, Port Douglas, Australia, 17–20 December 2002* (ed. K. Hourigan, T. Leweke, M. C. Thompson & C. H. K. Williamson). Monash University.

Vickery, B. J. & Watkins, R. D. 1964 Flow-induced vibrations of cylindrical structures. In *1st Australian Conf. on Hydraulics and Fluid Mechanics* (ed. R. Silvester). Pergamon.

Willden, R. H. J. & Graham, J. M. R. 2001 Numerical prediction of VIV on long flexible circular cylinders. *J. Fluids Struct.* **15**, 659–669.

Williamson, C. H. K. 1989 Oblique and parallel modes of vortex shedding in the wake of a cylinder. *J. Fluid Mech.* **206**, 579–628.

Williamson, C. H. K. 1996 Vortex dynamics in the cylinder wake. *Annu. Rev. Fluid Mech.* **28**, 477–526.

Williamson, C. H. K. & Govardhan, R. 2005 Vortex-induced vibrations. *Annu. Rev. Fluid Mech.* **36**, 413–455.

Williamson, C. H. K. & Roshko, A. 1988 Vortex formation in the wake of an oscillating cylinder. *J. Fluids Struct.* **2**, 355–381.

Wooton, L. R., Warner, M. H., Sainsbury, R. N. & Cooper, D. H. 1972 Oscillations of piles in marine structures. A resume of full-scale experiments at Immingham. *CIRIA Tech. Rep. 41.*